Geologia USP
Série Científica

https://doi.org/10.11606/issn.2316-9095.v20-151049

Revista do Instituto de Geociências - USP
Geol. USP, Sér. cient., São Paulo, v. 20, n. 4, p. 213-234, Dezembro 2020

Multiple processes of geochemical evolution for the alkaline rocks of Rio Bonito intrusive complex, Rio de Janeiro State, Brazil: $^{40}Ar/^{39}Ar$ and U-Pb ages and Lu-Hf isotopes on zircon and constraints on crustal signature

Múltiplos processos de evolução geoquímica para as rochas alcalinas do complexo intrusivo de Rio Bonito, Estado do Rio de Janeiro, Brasil: idades $^{40}Ar/^{39}Ar$ e U-Pb e isótopos Lu-Hf em zircão – considerações sobre assinatura crustal

Daniel Adelino da Silva[1], Akihisa Motoki[1†], Anderson Costa dos Santos[1], Julio Mendes[2], Fred Jourdan[3], Mauro César Geraldes[1], Cristiano de Carvalho Lana[4]

[1]Universidade do Estado do Rio de Janeiro - UERJ, Departamento de Mineralogia e Petrologia Ígnea, Rua São Francisco Xavier, 524, CEP 20550-900, Rio de Janeiro, RJ, BR (adelinogeologia@yahoo.com.br; geraldes@uerj.br; andcostasantos@gmail.com); [†]*in memoriam*.

[2]Universidade Federal do Rio de Janeiro - UFRJ, Instituto de Geociências, Rio de Janeiro, RJ, BR (julio@geologia.ufrj.br)

[3]University of Technology - GPO, Western Australian Argon Isotope Facility, Department of Applied Geology & JdL Centre, Curtin, Perth, Australia (f.jourdan@exchange.curtin.edu.au)

[4]Universidade Federal de Ouro Preto - UFOP, Isotope Geochemistry Laboratory, Ouro Preto, MG, BR (cristianodeclana@gmail.com)

Received on October 12, 2018; accepted on November 6, 2020

Abstract

This article presents geochemical characteristics of the alkaline rocks of Rio Bonito intrusive complex, State of Rio de Janeiro, Brazil, which is constituted mainly by nepheline syenite. The fractional crystallisation of this magma decreases $K_2O/(Na_2O + K_2O)$ and increases (Na + K)/Al. The TiO_2, Fe_2O_3*, MgO, CaO, and P_2O_5 contents indicate fractionation of titanite, ilmenite, and clinopyroxene or amphibole. The total rare earth elements (REEs) are high, and the REE pattern is linear with negative gradient. The nepheline syenite aplite has low REEs, concave REE pattern, and positive Eu anomaly. The ultrabasic and basic mela-nepheline syenite samples have total REEs and light REEs higher than the felsic alkaline rocks. Therefore, the nepheline syenite magma is not derived directly from the alkaline ultrabasic magma. Laser-spot step-heating $^{40}Ar/^{39}Ar$ ages for biotite and amphibole are 65.03 ± 0.70 and 65.03 ± 0.46. U-Pb ages LA-ICP-MS for two samples are 65.49 ± 0.30 and 65.18 ± 0.30. Values of ε_{Hf} are negative for both samples, indicating an important crustal component in the evolution of Rio Bonito.

Keywords: Nepheline syenite; Rio Bonito; Fractional crystallisation; Crustal assimilation; $^{40}Ar/^{39}Ar$ and U-Pb dating.

Resumo

Este artigo apresenta características geoquímicas das rochas alcalinas do complexo intrusivo de Rio Bonito, estado do Rio de Janeiro, Brasil, que é constituído principalmente por nefelina sienito. A cristalização fracionada desse magma diminui $K_2O/(Na_2O + K_2O)$ e aumenta (Na + K)/Al. Os conteúdos de TiO_2, Fe_2O_3*, MgO, CaO e P_2O_5 indicam fracionamento de titanita, ilmenita, clinopiroxênio e anfibólio. O total de terras raras é alto, e o padrão é linear com gradiente negativo. O nefelina sienito aplito tem concentrações de terras raras baixas com padrão côncavo e anomalia positiva de Eu. As amostras de mela-nefelina sienito ultrabásico e básico têm total de terras raras e terras raras leves maiores que as rochas alcalinas félsicas. Portanto, o magma nefelina sienítico não é derivado diretamente do magma alcalino ultrabásico. Idades $^{40}Ar/^{39}Ar$ *step-heating* para biotita e anfibólio são 65,03 ± 0,70 e 65,03 ± 0,46. Idades U-Pb LA-ICP-MS de duas amostras são 65,49 ± 0,30 e 65,18 ± 0,30. Os valores de ε_{Hf} são negativos para ambas as amostras, indicando um importante componente crustal na evolução de Rio Bonito.

Palavras-chave: Nefelina sienito; Rio Bonito; Cristalização fracionada; Assimilação crustal; Datação $^{40}Ar/^{39}Ar$ e U-Pb.

INTRODUCTION

In the southeastern Brazilian coast region, there is a suit of felsic alkaline intrusive bodies dated from Cretaceous to Early Cenozoic (Figure 1), such as: Itatiaia (Brotzu et al., 1997), Morro Redondo (Brotzu et al., 1989), Tinguá, Mendanha, Marapicu (Motoki et al., 2007a; Silva et al., 2015), Itaúna (Motoki et al., 2008c), Tanguá, Soarinho, Rio Bonito (Motoki et al., 2010), Morro dos Gatos (Motoki et al., 2012a; Geraldes et al., 2013a), Cabo Frio Island (Sichel et al., 2008; Motoki et al., 2013), and Morro de São João (Brotzu et al., 2007; Mota et al., 2009; Geraldes et al., 2013b). These stocks form a WNW-ESE trend called Poços de Caldas-Cabo Frio magmatic alignment (Sadowski and Dias Neto, 1981), and are constituted mainly by nepheline syenite and alkaline syenite. The syenitic stocks are cross-cut by dykes of phonolite, trachyte, and lamprophyre. Some of them have strongly welded and secondary-flowed vent-filling subvolcanic tuff breccia, such as happen in Itatiaia, Mendanha, Itaúna, Morro dos Gatos, and Cabo Frio Island (Motoki et al., 2007c, 2008b; Mota and Geraldes, 2006). The intrusive depth is estimated to be 3 km based on the geologic mode of occurrence and fission track in apatite (Motoki et al., 2007b, 2008a; Motoki and Sichel, 2006, 2008). This alkaline alignment has been evoked to constraint the influence of Trindade Plume based on chemistry and isotopes signature according to Thompson et al. (1998) and references therein.

According to Motoki et al. (2010, 2013) and Sichel et al. (2012), the chemical variation for the mafic alkaline rocks originate from mafic minerals fractionation, whereas for the felsic alkaline rocks originate from leucite and K-rich alkaline feldspar fractionation. The fractionation of the felsic alkaline magmas decreases $K_2O/(Na_2O + K_2O)$. In addition, the above-mentioned authors presented evidences of strong effects of continental crust assimilation based on Silica Saturation Index (SSI). The SSI is a geochemical parameter calculated from all of the major oxides but TiO_2 and P_2O_5 divided by its molecular masses. Rocks with positive SSI are SiO_2-oversaturated, and those with negative SSI are SiO_2-undersaturated. The gradual passage from SiO_2-undersaturated rocks to the SiO_2-oversaturated ones within the same intrusive body, crossing over the

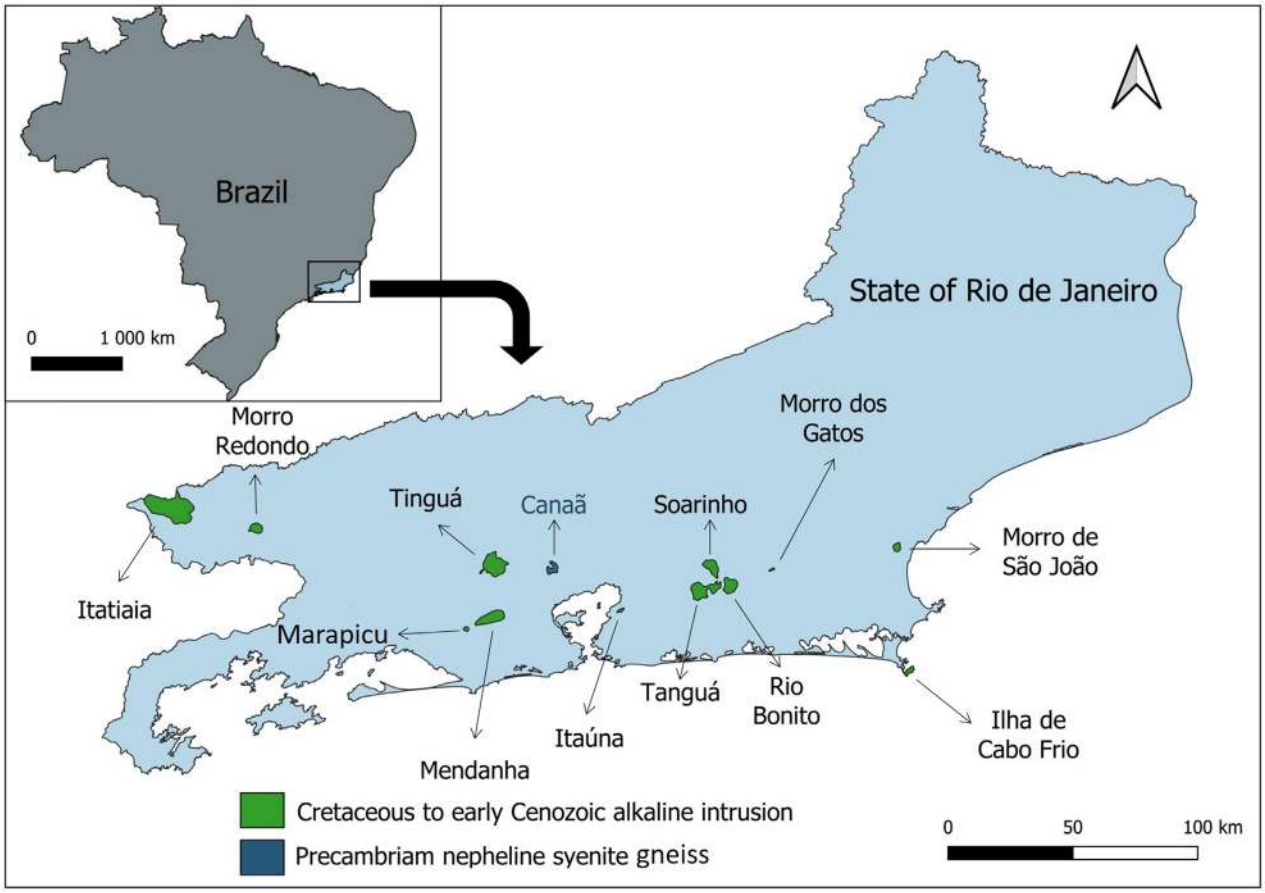

Figure 1. Distribution map for the felsic alkaline bodies of State of Rio de Janeiro. With the exception of Canaã complex, which is Cambrian nepheline syenite gneiss, they are Cretaceous to early Cenozoic intrusive bodies.

thermal divide between nepheline and quartz, is a peculiar phenomenon.

This article presents the results and considers the geochemical evolution of the nepheline syenite magma of Rio Bonito intrusive complex. The authors performed fieldwork, lithologic and petrographic observations, geochemical analyses, $^{40}Ar/^{39}Ar$ laser-spot step-heating datings, U-Pb datings and Lu-Hf analyses for the alkaline rocks of Rio Bonito intrusive complex, situated in the central region of Rio de Janeiro state, Brazil. The new data indicates the geochemical effects of fractional crystallization and continental crust influence based on silica saturation index calculated according to the form proposed by Motoki et al. (2010) and Sichel et al. (2012). U-Pb and Lu-Hf isotopes were performed using laser ablation inductively coupled plasma mass spectrometer (LA-ICP-MS) in zircons and provided crucial information about melt provenance once U-Pb dating performed in zircon grains can give precise crystallization ages whereas epsilon hafnium (ε_{Hf}) records the degree to which a melt incorporates juvenile mantle versus reworked preexisting crust sources (Bataille et al., 2017). We also present here the SSI proposed by Motoki et al. (2010) and Sichel et al. (2012) as a good parameter to indicate continental crust provenance instead of contamination as previously suggested by those authors.

RIO BONITO INTRUSIVE COMPLEX

The Rio Bonito intrusive complex occurs at 22°40'S, 42°38'W, about 65 km to the east-northeast of the city of Rio de Janeiro, Brazil. The distribution area of alkaline rocks is about 7 (NE-SW) × 6 km (NW-SE), forming an outstanding massif with approximate relative height of 900 m. The Tanguá and Soarinho intrusive complexes occur very close to Rio Bonito intrusive body (Figure 1).

The basement of the alkaline intrusion is composed mainly of Cambrian orthogneiss and paragneiss of the Pan-African continental collision event (e.g. Heilbron and Machado, 2003; Schmitt et al., 2004), with metamorphic ages of 510 to 550 Ma. The metamorphic basement is cut by post-tectonic granite dykes (Valeriano et al., 2011) and silicified tectonic breccia of the late stage of the continental collision event (Motoki et al., 2011, 2012b). They are cut by early Cretaceous mafic dykes intruded by hydraulic shear fracturing (Motoki et al., 2009), which correspond to a part of feeder dykes of the Paraná continental flood basalt (Stewart et al., 1996).

The Rio Bonito complex shows similar geologic mode of occurrence to the other felsic alkaline bodies of the Poços de Caldas-Cabo Frio alignment. The stock is constituted mainly by nepheline syenite and alkali feldspar syenite. Similar to the case of Tanguá complex, trachytic and phonolitic dykes are scarce, and in the northeastern border, welded subvolcanic tuff breccia is present. The Figure 2 shows sampling site map and indicates the distribution area of felsic alkaline rocks of Rio Bonito complex is much wider than the previous mapping (Heilbron et al., 2016).

ANALYTICAL TECHNIQUES

Whole-rock chemistry

The chemical analyses for the alkaline rocks of Rio Bonito intrusive complex have been performed in the Acme Laboratories Ltd., Ontario, Canada, using XRF and ICP-MS (Table 1). The detection limit for the major elements is 0.01% except for MnO and TiO_2 (0.001%); for the trace elements, detection limits range from 0.1 to 30 ppm.

$^{40}Ar/^{39}Ar$ analyses

The analytical procedures were performed at Laeter John Centre for Isotope Research, Curtin University (Australia). K and Ar isotope abundances were obtained by mass spectrometry. The procedures include neutron activation to transform ^{40}K into ^{39}Ar and step-heating fusion of the whole sample. After the analytical process, two values are obtained for ages:

- plateau age, using criteria of Dalrymple and Lanphere (1974);
- isochron age, with isotopic data extracted from each step of fusion of the same sample.

Correction for atmospheric Ar ($^{40}Ar/^{36}Ar = 295.5$) was also performed. The probability of success of the plateau/isocronic ages is done by examining the Pearson's chi-square (χ^2) distribution (Wendt and Carl, 1991). This statistical method uses as input parameters the values of mean squared weighted deviation (MSWD) and the number of steps that define the plateau or the points that define the isochron age.

U-Pb dating by LA-ICP-MS

Two nepheline syenite samples (Rb-01 and Rb-02) were dated by U-Pb using a LA-ICP-MS. The analyses were made at Isotope Geochemistry Laboratory from Universidade Federal de Ouro Preto, Brazil. Zircon grains from these samples were separated using conventional heavy liquid and magnetic techniques, and the grains were handpicked under a binocular microscope to ensure purity. These zircon grains were mounted onto an epoxy resin disc, polished to about half of the zircon modal grain thickness and coated with gold film. Zircons were documented with Scanning Electron Microscope (SEM) images to reveal their external

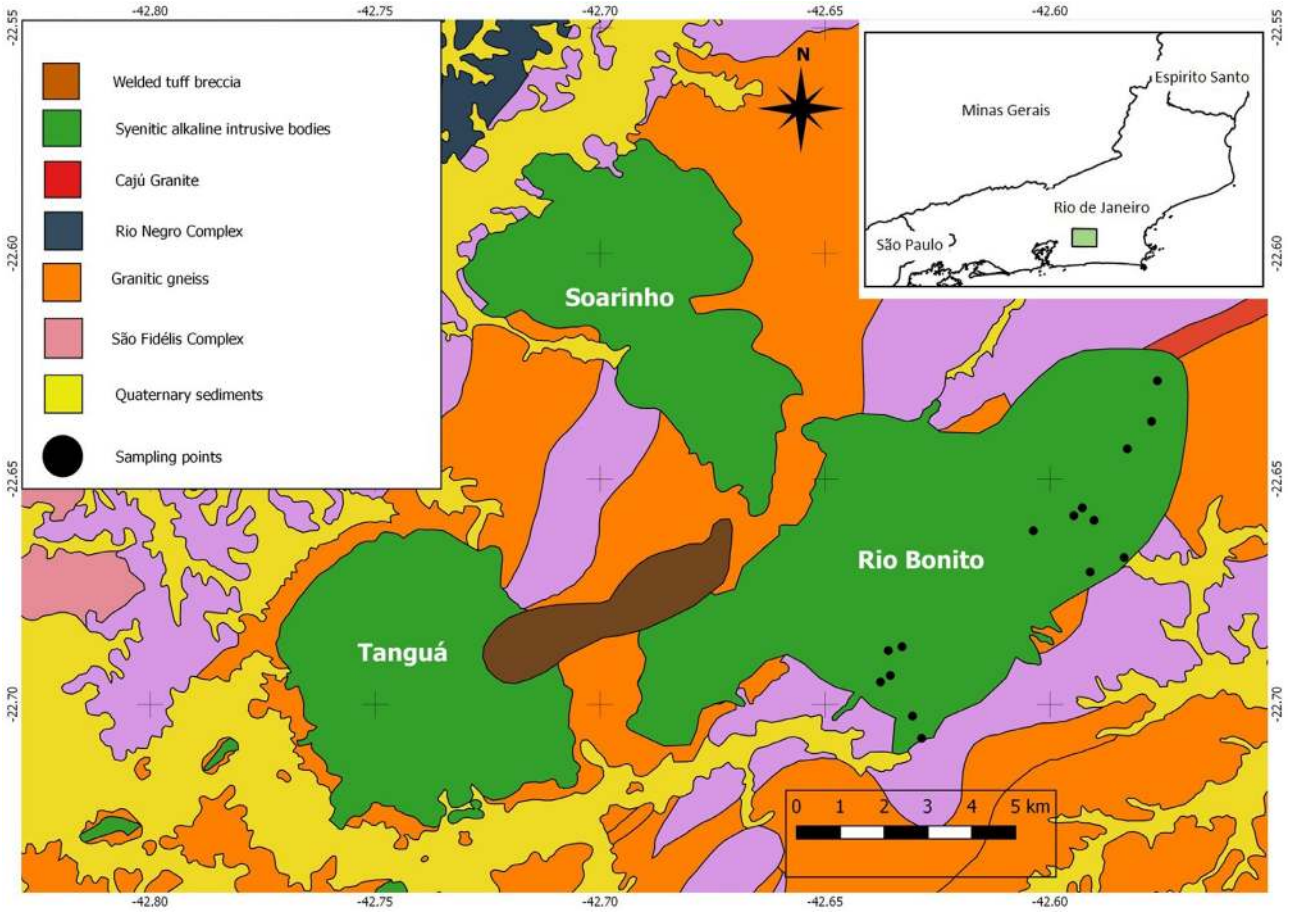

Figure 2. Geologic map for intrusive complex of Rio Bonito, Tanguá, and Soarinho showing sampling sites.

Table 1. New geochemical analyses for the samples of Rio Bonito intrusive complex. Fe_2O_3* corresponds to total iron as ferric.

	RIB01-A	RIB01-C	RIB01-D	RIB02-B	RIB03	RIB04	RIB05-A	RIB05-B	RIB06-A	RIB06-B	RIB07-A
	Ns	Ns	Ns	Ns	Ns	Ns	Ns	Ns	Ns	Ns	Ns
SiO_2	56.24	58.86	56.61	55.9	57.69	56.37	55.31	55.36	57.1	58.51	54.57
TiO_2	1.27	0.45	0.61	1.52	0.78	1.24	1.42	1.44	1.14	0.72	1.39
Al_2O_3	19.21	20.96	21.37	18.47	18.7	18.66	18.95	18.33	18.64	18.83	18.2
Fe_2O_3*	3.89	1.62	2.27	4.88	2.94	3.73	4.73	4.81	3.36	2.65	4.65
MnO	0.19	0.08	0.12	0.18	0.12	0.16	0.18	0.19	0.24	0.17	0.18
MgO	0.86	0.19	0.32	1.22	0.68	0.83	1.02	1.13	0.7	0.38	1.15
CaO	2.76	1.23	1.61	3.36	2.13	2.93	3.19	3.26	2.29	1.76	3.08
Na_2O	4.27	5.81	6.2	3.98	3.96	4.04	4.86	4.98	4.9	4.49	4.08
K_2O	8.34	9.05	8.5	8.17	8.8	8.33	7.94	7.62	8.22	8.44	7.88
P_2O_5	‘’	0.05	0.1	0.45	0.24	0.31	0.35	0.37	0.09	0.09	0.39
LOI	2.12	1.25	1.62	1.86	1.75	2.35	2.28	1.58	1.55	2.27	2.47
Total	97.32	98.3	97.71	98.13	96.04	96.59	97.95	97.48	96.68	96.05	95.57
Rb	117	118	121	96	99	101	111	98	109	123	104
Sr	2547	601	1429	2036	2160	2047	1199	1269	242	411	1748
Ba	222	34	62	354	503	369	72	91	7	64	274
Zr	301	531	2203	331	216	366	437	354	430	422	369
Y	52	19	30	40	15	35	38	39	57	49	35

Continue...

Table 1. Continuation.

	RIB01-A	RIB01-C	RIB01-D	RIB02-B	RIB03	RIB04	RIB05-A	RIB05-B	RIB06-A	RIB06-B	RIB07-A
	Ns	Ns	Ns	Ns	Ns	Ns	Ns	Ns	Ns	Ns	Ns
Nb	204	94	122	117	59	125	125	131	272	191	118
Th	9.8	8.7	23.3	7.1	5.4	8.9	8.8	7.6	11.8	12.3	9.1
U	1.7	2	6.2	1.6	1.3	2.1	1.9	1.7	2.4	3.1	2.2
Pb	10	10	12	9	9	10	9	9	12	13	10
Zn	130	60	90	140	90	120	140	140	150	110	150
Ag	1.1	2.1	9.8	1.2	0.8	1.4	1.8	1.3	1.6	1.7	1.5
Be	2	2	4	2	2	2	2	2	2	2	2
Co	2	1	2	2	1	2	2	2	2	2	2
Mo	8	5	3	5	4	6	5	3	7	11	4
Sc	1	N.A.	N.A.	3	2	2	2	3	2	1	3
Cs	0.7	0.5	1.1	0.7	0.6	1	0.8	0.7	0.7	0.9	0.9
Hf	8.9	8.6	29.6	8.7	4.9	9	10	9.4	12.6	11.1	9.4
Ta	20.1	7.7	9.4	9.6	4.1	9.5	9.9	10.1	24.7	17.8	9.3
Ga	23	22	27	22	19	22	23	22	25	24	23
La	204	98	133	166	93.9	156	162	165	250	194	155
Ce	428	184	250	326	158	297	314	317	517	378	298
Pr	52.5	19.9	27.4	42.1	18.1	37.5	39.6	39.8	64.4	45	37.7
Nd	183	63	90.2	160	63.4	137	146	148	213	149	141
Sm	27.4	8.4	12.4	24.9	9.3	21.3	23.1	23.4	28.6	20.4	22.3
Eu	8.53	2.81	4.43	9.82	5.99	8.61	8.7	9.04	6.48	5.51	8.69
Gd	17.2	5.1	7.8	15.6	5.8	13	14.3	14.7	16.3	13.2	13.7
Tb	2.3	0.7	1.1	2	0.7	1.7	1.8	1.8	2.4	1.8	1.8
Dy	11.3	3.8	5.6	9.4	3.5	8.2	9	8.9	12.3	9.8	8.6
Ho	1.9	0.7	1.1	1.5	0.6	1.3	1.5	1.5	2.2	1.8	1.5
Er	5	1.9	3.1	3.9	1.6	3.5	3.8	3.8	5.9	5	3.6
Tm	0.6	0.25	0.45	0.47	0.2	0.42	0.47	0.46	0.74	0.68	0.44
Yb	3.2	1.5	3.2	2.5	1.1	2.3	2.6	2.6	3.8	4	2.4
Lu	0.41	0.23	0.55	0.34	0.15	0.32	0.35	0.35	0.49	0.58	0.32

	RIB08-C	RIB13	RIB14-A	RIB14-B	RIB15-A	RIB15-B	RB-6	Rb-5	Rb-7	Rb-8	R-4	Rb-3
	Ns	Ns	Ns	Ns	Ns	Ns	Ap	Ap	Wt	Wt	Ba	Ub
SiO_2	54.35	57.23	56.82	58.8	58.36	57.8	56.37	55.13	58.77	58.77	47.68	44.22
TiO_2	0.32	1.02	1.11	0.94	0.82	0.77	0.16	0.16	0.58	0.59	2.86	3.38
Al_2O_3	22.12	19.22	19.28	18.86	18.94	18.36	22.36	23.39	19.46	20	16.89	15.52
$Fe_2O_3^*$	1.65	3.53	3.73	3.02	2.85	2.82	1.33	0.99	3.02	3.01	9.87	11.77
MnO	0.09	0.17	0.18	0.21	0.19	0.18	0.09	0.06	0.03	0.03	0.6	1
MgO	0.15	0.66	0.69	0.53	0.44	0.43	0.05	0.05	0.21	0.2	2.15	1.6
CaO	1.25	2.23	2.35	1.98	2.02	1.79	0.88	0.97	0.44	0.4	5.58	8.32
Na_2O	7.61	5.16	5.2	4.44	5.36	5.35	6.78	7.67	4.09	4.15	4.61	7.58
K_2O	7.51	8.25	8.05	8.8	7.8	8.02	8.35	7.79	6.99	7.22	5.93	3.36
P_2O_5	0.04	0.21	0.21	0.11	0.09	0.08	0.02	0.02	0.14	0.14	0.71	0.48
LOI	2.72	2.37	2.33	4.57	4.86	3.71	2.28	2.29	2.55	2.05	3.27	3.01
Total	95.09	97.68	97.61	97.69	96.87	95.59	96.38	96.23	93.74	94.51	96.89	97.22
Rb	147	130	121	122	150	144	133	131	160	165	98	113
Sr	407	811	695	430	226	266	176	161	93	92	785	146
Ba	63	59	42	60	17	28	7	12	44	46	112	20
Zr	274	572	594	555	610	433	860	827	1109	1189	1026	2662
Y	15	31	33	50	36	31	6	5	53	69	127	154
Nb	131	131	129	227	178	152	69	53	199	190	528	N.A.
Th	13.2	10.2	11.4	14.4	21	17.1	32.1	21.5	19	20.8	26.1	159
U	2	2	2.8	2.7	5.4	3.8	10.9	6.8	4.7	5.3	5.6	17.6
Pb	11	12	11	11	18	15	20	13	19	22	11	10

Continue...

Table 1. Continuation.

	RIB08-C	RIB13	RIB14-A	RIB14-B	RIB15-A	RIB15-B	RB-6	Rb-5	Rb-7	Rb-8	R-4	Rb-3
	Ns	Ns	Ns	Ns	Ns	Ns	Ap	Ap	Wt	Wt	Ba	Ub
Zn	60	110	110	120	110	100	80	60	110	80	400	500
Ag	1.1	2.3	2.3	2.2	2.6	1.6	4	3.4	4.4	5.1	4.5	12
Be	3	2	3	2	5	3	10	6	3	3	4	8
Co	1	2	2	2	2	2	1	1	2	2	3	5
Mo	5	4	3	12	3	2	N.A.	N.A.	N.A.	N.A.	12	N.A.
Sc	N.A.	2	2	1	1	1	N.A.	N.A.	5	5	5	4
Cs	1.3	0.5	0.9	0.7	1.7	1.9	3.7	2.1	1.5	1.3	1	1.5
Hf	6.4	11.6	12	12.7	14.8	10.9	17.1	13.2	22.5	23.3	28.6	63
Ta	10.1	8.5	9.4	21.9	12.1	10.3	1.5	1.6	12.6	13.1	49.8	98.6
Ga	26	25	24	23	26	24	33	31	29	30	36	47
La	115	147	146	216	172	153	112	67.1	251	278	508	1280
Ce	193	263	273	457	293	262	93	63.2	494	559	1020	2020
Pr	17.4	28.7	31	53.8	30.5	26.8	4.9	3.86	52.3	58.4	127	186
Nd	46.7	100	110	177	101	85.1	10.4	8.5	171	201	435	487
Sm	5.4	15.3	17	23.8	14.9	12	1	0.8	25.1	30.2	62.5	55.8
Eu	1.35	5.93	6.31	5.84	3.85	3.31	0.6	0.53	4.81	5.82	14.7	11.5
Gd	3.4	10.1	11.1	14.6	10	8.2	1	0.5	16.2	21.6	39.4	37.5
Tb	0.5	1.3	1.4	2	1.4	1.1	0.1	N.A.	2.2	2.9	5.3	5.1
Dy	2.7	6.3	7	10.4	7.3	6.1	0.7	0.6	11.2	13.9	26.6	27.8
Ho	0.5	1.1	1.2	1.9	1.3	1.1	0.2	0.1	2	2.5	4.7	5.3
Er	1.5	3.1	3.3	5.1	3.6	3.1	0.7	0.5	5.4	6.6	12.6	15.9
Tm	0.22	0.41	0.42	0.64	0.49	0.41	0.14	0.12	0.74	0.89	1.59	2.22
Yb	1.3	2.5	2.5	3.5	3.1	2.6	1.2	1	4.6	5.4	8.7	13.4
Lu	0.19	0.36	0.37	0.48	0.46	0.38	0.24	0.2	0.71	0.81	1.21	2.09

Ns: nepheline syenite and nepheline-bearing alkaline syenite; Ap: nepheline syenitic aplite; Wt: welded lapilli tuff; Ub: ultrabasic mela-nepheline syenite; Ba: basic mela-nepheline syenite.

and internal structures. The data were selected to ensure discordance less than 5%, and low common lead. The data are presented in Tera and Wasserburg (1972) Concordia constructed by using Isoplot program (Ludwig, 2003).

Lu-Hf isotopes in zircons

Zircon Lu-Hf isotopes were obtained from the original locations of the LA-ICP-MS analyses. Zircons constrain important tool analysing those heavy isotopes once they do not fractionated from each other during magmatic processes and can imprint the melts signature from which they crystalized. Those analyses were made at Isotope Geochemistry Laboratory from Universidade Federal de Ouro Preto, Brazil.

Lithologic and petrographic characteristics

Most of the constituent rocks of Rio Bonito complex are nepheline syenite and nepheline-bearing alkali feldspar syenite (Figure 3A). In general, no mineral orientation and cumulative texture are observed. Some samples contain alkaline feldspar phenocrysts with typical size of 2.5 × 1 cm (Figure 3B). About 80% in volume of the constituting minerals are intermediate alkaline feldspar showing micro-interlocking perthite. Nepheline is slightly pinkish and occurs in the interstitial space of alkaline feldspar framework and generally altered into analcime. Mafic mineral is amphibole with subordinate amount of biotite. The presence of titanite is notable (Figure 4A). Apatite and zircon occur as accessory minerals. Veins of nepheline syenite aplite of 10 to 20 cm in width are commonly found. The grain size of the aplite ranges from 0.1 (Figure 4B) to 1 mm (Figure 3C).

There are two samples of coarse-grained rocks with abundant mafic minerals (Figure 3D) which are constituted by alkaline feldspar, nepheline, clinopyroxene, amphibole, and titanite (Figure 4C). The clinopyroxene is euhedral showing zoning and nepheline is generally altered into analcime. These rocks have mineralogical composition of nepheline syenite and, due to its high amount of mafic minerals and chemical composition, in this paper, the authors classify samples Rb-3 and Rb-4, respectively, ultrabasic mela-nepheline syenite and basic mela-nepheline syenite. Such classification is in accordance with IUGS recommended nomenclature for igneous rocks (Le Maitre, 2002). Similar alkaline

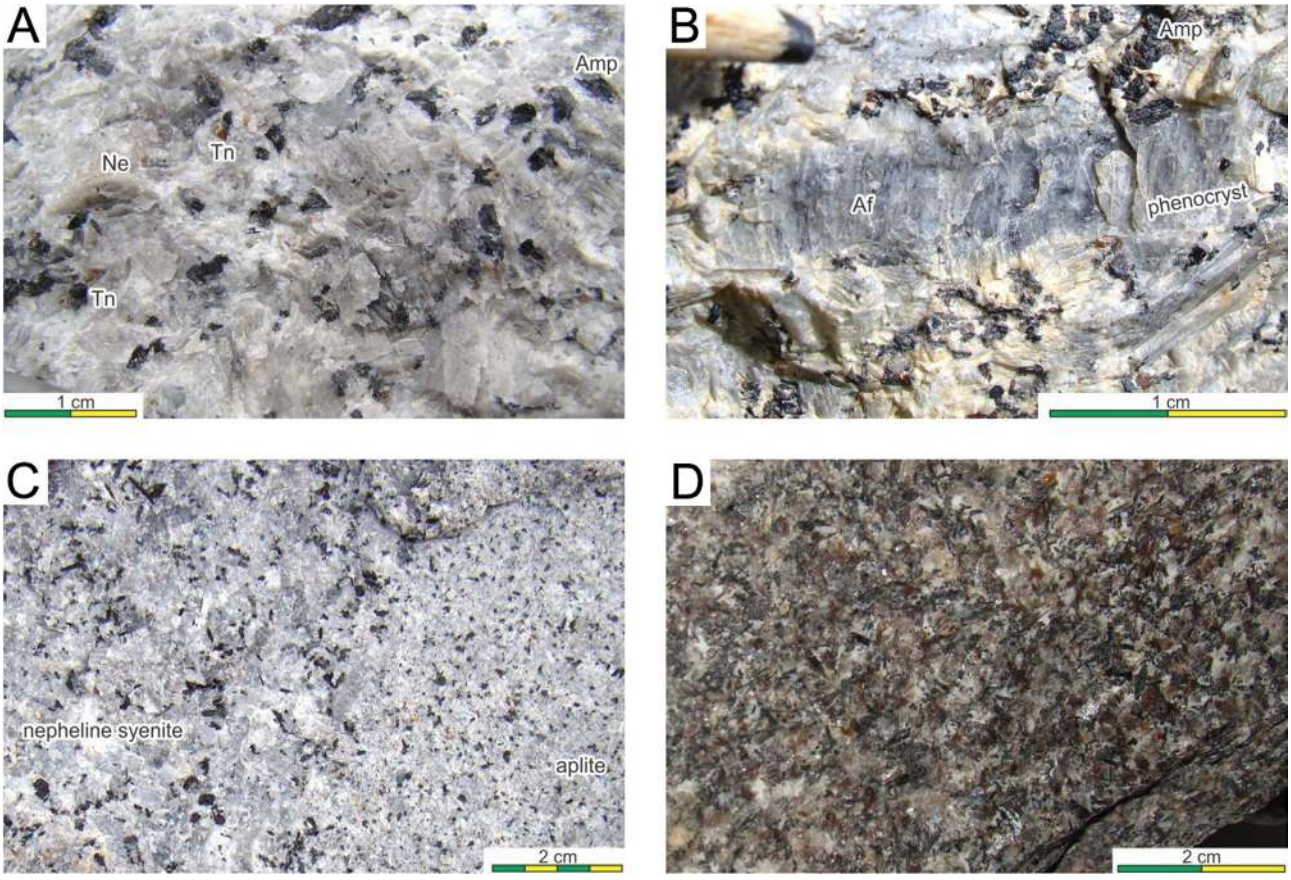

Af: alkaline feldspar; Amp: amphibole; Ne: nepheline; Tn: titanite.

Figure 3. Akaline rocks of Rio Bonito complex. (A) Nepheline syenite, RIB-01; (B) nepheline syenite with alkaline feldspar phenocryst, RIB-13; (C) nepheline syenite aplite, Rb-6; (D) ultrabasic mela-nepheline syenite, Rb-3.

mafic rocks are found as enclaves captured by nepheline syenite in the intrusive bodies of Morro de São João, Cabo Frio Island, and São Sebastião Island.

A gravel of welded lapilli tuff of 30 × 15 cm in size is found in a stream bottom. This rock contains angular fragments of trachyte and syenite smaller than 2 cm (Figure 4D). The mineral grains smaller than 0.1 mm have highly fragmented shape. The matrix texture indicates high-grade welding and strong secondary flow. Because of the advanced plastic deformation, flattened lens-shaped essential fragments are no more observable. These textural characteristics are common in vent-filling subvolcanic welded tuff breccia, observed in the alkaline intrusive complexes of Morro Redondo, Mendanha, Itaúna, Tanguá, Morro dos Gatos, and Cabo Frio Island (Brotzu et al., 1989; Motoki et al., 2007b, 2007c, 2008b, 2008c; Sichel et al., 2008). The limited field occurrence suggests that the welded tuff breccia could be originated from a pyroclastic dyke as seen in Mendanha and Morro dos Gatos complexes (Motoki et al., 2007a, 2012a). Samples RIB-01, RIB-07, and RIB-08 of Rio Bonito are constituent of trachyte dyke and trachytic subvolcanic pyroclastic conduit and fissure.

Major and trace elements

The classification diagram of Le Bas et al. (1986) shows that all of the analysed samples plot on the areas of alkaline rocks (Figure 5). Most of the rocks are felsic and their SiO_2 contents range from 52.43 to 61.72 wt% (Table 1).

The ultrabasic and basic mela-nepheline syenite of the Rio Bonito complex have differentiation index (D.I. Thornton and Tuttle, 1960) respectively of 69.23 and 55.47 wt%, which are significantly lower than the felsic alkaline rocks, with average value of 89.93 wt%. They have high normative nepheline contents respectively 15 and 30 wt%, being plotted on the tephri-phonolite field (Figure 5). The ultrabasic mela-nepheline syenite has exceptionally 2.66 wt% of normative acmite, although the other rocks of Rio Bonito have none.

The nepheline syenite aplite have high normative nepheline content constitution, respectively 20.22 and 25.41 wt%

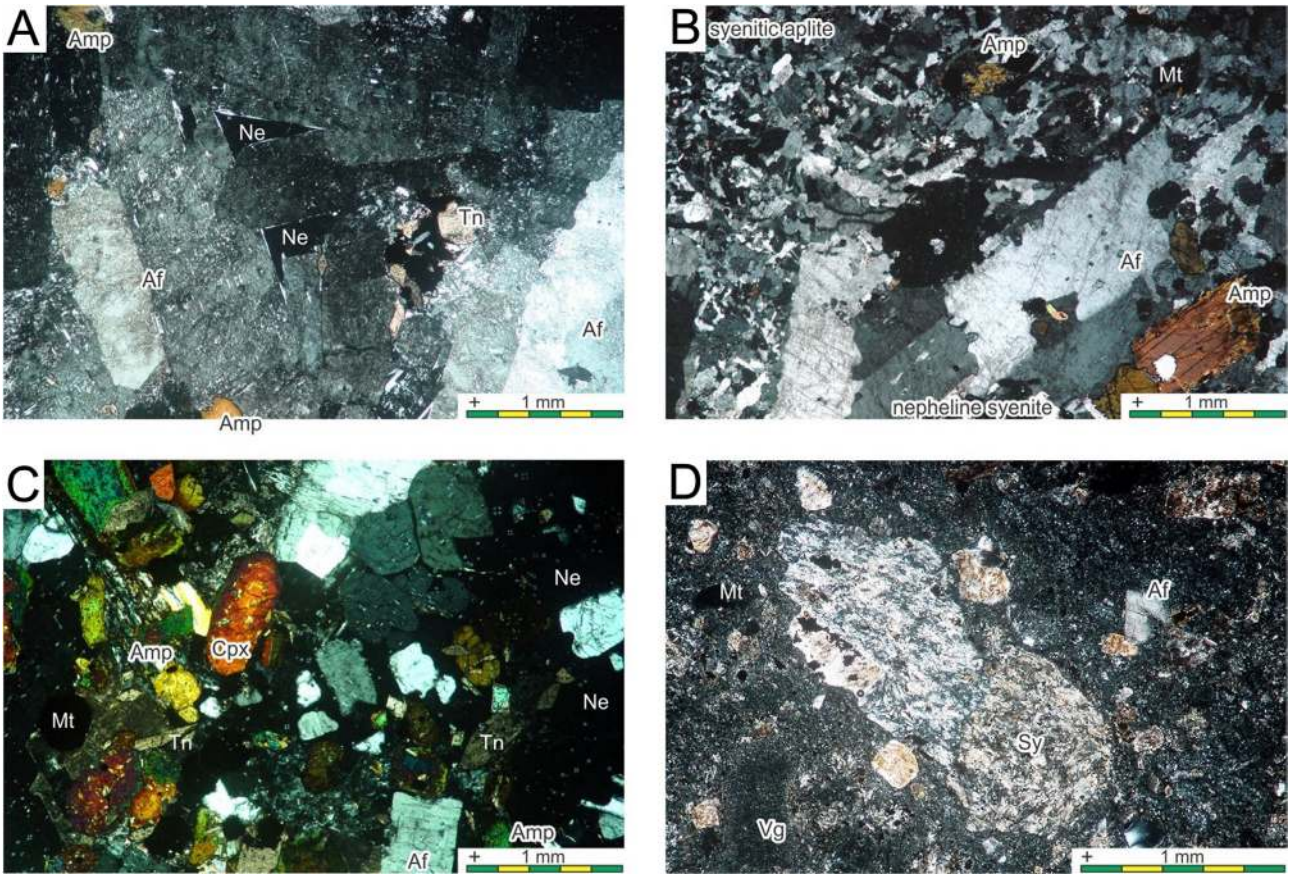

Af: alkaline feldspar; Amp: amphibole; Ne: nepheline altered into analcite; Cpx: clinopyroxene; Mt: magnetite; Tn: titanite; Sy: syenitic rock (accidental fragment).

Figure 4. Photomicrography of the alkaline rocks of Rio Bonito intrusive complex. (A) Nepheline syenite, RIB-13; (B) syenitic aplite, Rb-6; (C) ultrabasic mela-nepheline syenite, Rb-3; (D) welded lapilli tuff, RIB-08. The symbol + means crossed polarizer.

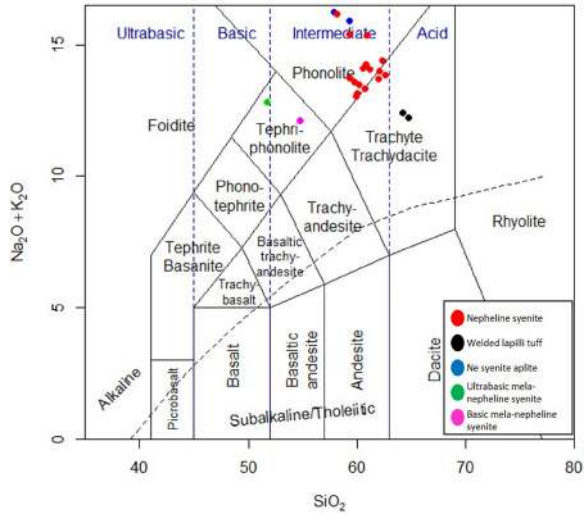

Figure 5. $Na_2O + K_2O$ vs. SiO_2 (wt%) diagram for the alkaline rocks of Rio Bonito complex. The classification nomenclature is after Le Bas et al. (1986). Limit between alkaline and non-alkaline rocks defined by Irvine and Baragar (1971).

and normative corundum of 0.62 wt%. These rocks are potassic, with respective $K_2O/(K_2O + Na_2O)$ ratio of 0.50 and 0.55. No normative clinopyroxene is found. Their differentiation indexes are notably high, 94.74 and 94.47 wt%, respectively.

The diagram of Na_2O vs. K_2O shows that the felsic alkaline rocks have high total alkalis and the K_2O is higher than Na_2O (Figure 6A). Most of the rocks of Rio Bonito complex are ultrapotassic or potassic (Figure 6A).

The alkali-alumina diagram (Figure 6B) shows that highly fractionated felsic rocks tend to be peralkaline and most of felsic alkaline rocks of Rio Bonito complex are less fractionated and have no normative acmite. Trachytic rocks of Rio Bonito are peraluminous. The ultrabasic and basic mela-nepheline syenite are peralkaline and metaluminous, respectively.

The good linear convergence on the diagrams of MgO + Fe_2O_3* vs. CaO and SiO_2 vs. CaO, with respective R^2 of 0.895 and 0.629, is attributed to fractionation of clinopyroxene and amphibole (Figure 7).

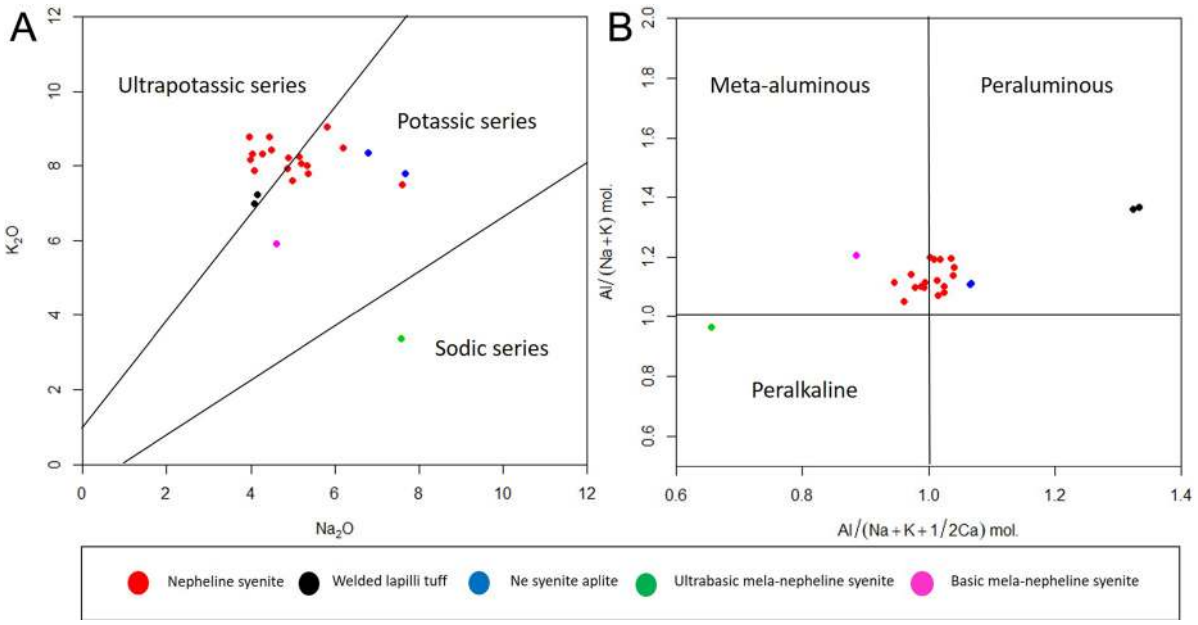

Figure 6. Geochemical classification diagrams for the alkaline rocks of Rio Bonito intrusive complex. (A) Na_2O vs. K_2O wt% according to Middlemost (1975); (B) Alkali-alumina saturation diagram after Maniar and Piccoli (1989).

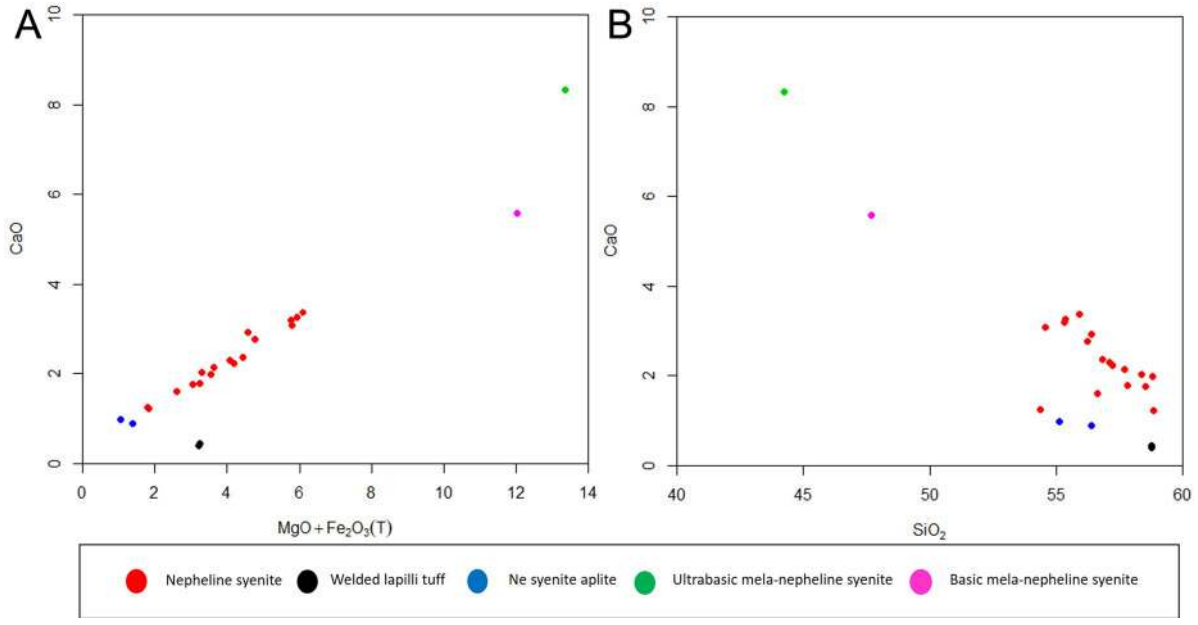

Figure 7. Geochemical effects of mafic mineral fractionation represented by MgO, Fe_2O_3*, and CaO for Rio Bonito alkaline complex. (A) MgO + Fe_2O_3* vs. CaO wt%; (B) SiO_2 wt% vs. CaO wt%.

The TiO_2 vs. Fe_2O_3* diagram exhibits well-converged positive correlation with $R^2 = 0.839$, suggesting strongly ilmenite fractionation (Figure 8A). The positive correlations on the diagrams of TiO_2 vs. CaO and TiO_2 vs. P_2O_5, with respective R^2 of 0.924 and 0.635, indicate titanite fractionation (Figures 8B and 8C), which is common in these alkaline rocks.

The large ion lithophile elements (LILE) ratios cannot express well the fractional crystallization processes of the studied rocks. The wide range of the Rb/Ba and Rb/Sr ratios suggests a strong signature of continental crust in the intrusive bodies. The concentrations of Ba and Sr have a positive correlation (Figure 9).

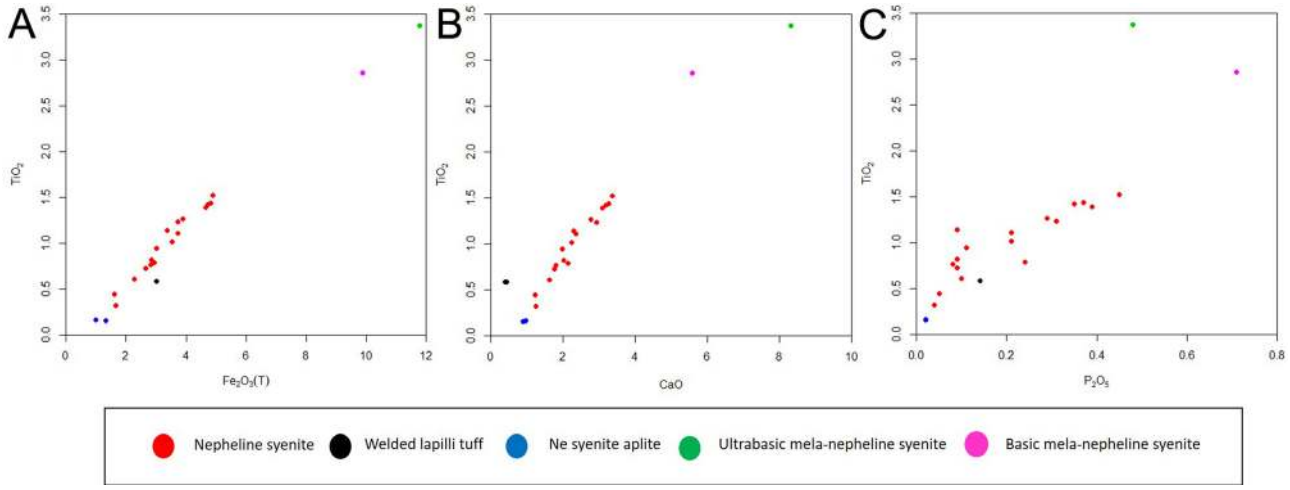

Figure 8. Variation diagrams in relation to titanium. (A) Fe_2O_3* vs. TiO_2 wt%; (B) CaO vs. TiO_2 wt%; (C) P_2O_5 vs. TiO_2 wt%.

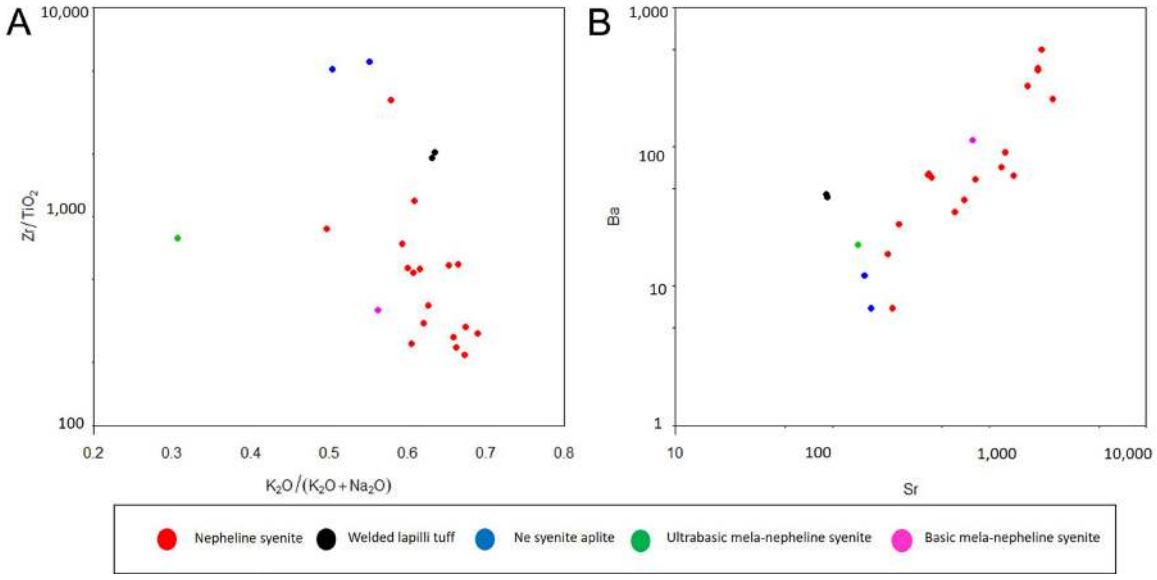

Figure 9. Variation diagrams for Zr, Sr, and Ba showing fractional crystallization process. (A) $K_2O/(K_2O + Na_2O)$ vs. Zr/TiO_2; (B) Sr vs. Ba.

The Figure 10 shows C1 chondrite normalized rare earth elements (REE) of the alkaline rocks of Rio Bonito. The average total REEs of the felsic rocks of Rio Bonito complex is 646 ppm, which is similar to that of Tanguá complex, 703 ppm, and about twice of Morro de São João, 333 ppm. The REE patterns are characterised by enrichment of light RREs. The average La_N/Yb_N (CI chondrite normalized values) of the felsic rocks of Rio Bonito complex is 43.6, which is similar to Tanguá, 49.1, and almost double of Morro de São João, 29.1. The average La_N/Sm_N of the felsic rocks of Rio Bonito, Tanguá, and Morro de São João is, respectively, 9.63, 6.34, and 11.28. Most of the samples have almost linear REE variation pattern from La to Yb. However, the nepheline syenite aplites of Rio Bonito show concave-up pattern with low total REEs.

On the other hand, total REEs concentration of the ultrabasic and basic mela-nepheline syenite of Rio Bonito complex, respectively 2,267 and 4,150 ppm, is much higher than that of the felsic alkaline rocks. They are about 4 times of

alkaline ultrabasic and basic rocks of Morro de São João body, 837 ppm in average.

The Figure 11 shows primitive mantle normalised multi-elements spider diagrams comparing LILE and high field-strength elements (HFSE). The Sr, Ba, and P shows strong negative anomalies, being 10 to 100 times lower than the adjacent elements. The negative anomaly variation of Sr and Ba is of wide range. Some felsic rocks of Rio Bonito show notable negative anomaly of Sm and Y.

Geochronology

$^{40}Ar/^{39}Ar$ laser-spot dating

Two nepheline syenite samples (RIB01-B and RIB01-A) of Rio Bonito complex have been submitted to laser-spot step-heating $^{40}Ar/^{39}Ar$ dating. The samples selected for the dating are highly SiO_2-undersaturated rock to avoid xenocrysts originated form the wall rock. The dating for biotite of the sample RIB01-B shows a coherent plateau of 65.03 ± 0.70 Ma with MSWD of 0.48 (Figure 12A). The amphibole of the sample RIB01-A demonstrates a plateau of 65.03 ± 0.46 Ma with MSWD of 0.09 (Figure 12B). The coherent plateaus endure high accuracy of the datings.

These $^{40}Ar/^{39}Ar$ ages are close to the Rb-Sr whole rock age of adjacent intrusive complex of Tanguá, 66.8 Ma (Motoki et al., 2010). These ages are according to the general tendency of alkaline intrusive body of Poços de Caldas-Cabo Frio magmatic alignment whose ages become younger from west to east.

U-Pb and Lu-Hf performed in zircon grains

Twenty-eight laser spots were made for each sample. Sample RB-01 shows a concordant age of 65.47 ± 0.6 Ma

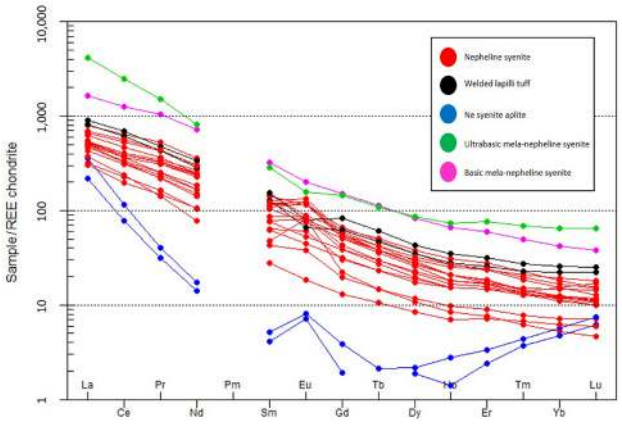

REE: rare earth elements.

Figure 10. Normalised rare earth elements for the alkaline rocks of Rio Bonito complex. The CI chondrite data are from Boynton (1984).

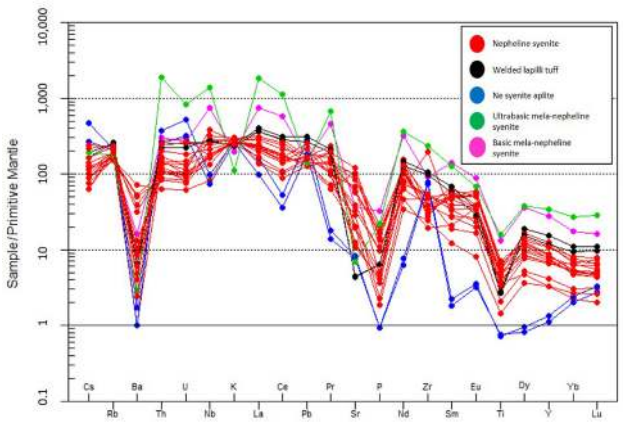

Figure 11. Primitive mantle normalised multi-elements spider diagrams contrasting large ion lithophile elements and high field-strength elements. The data of primitive mantle are after Sun and McDonough (1989).

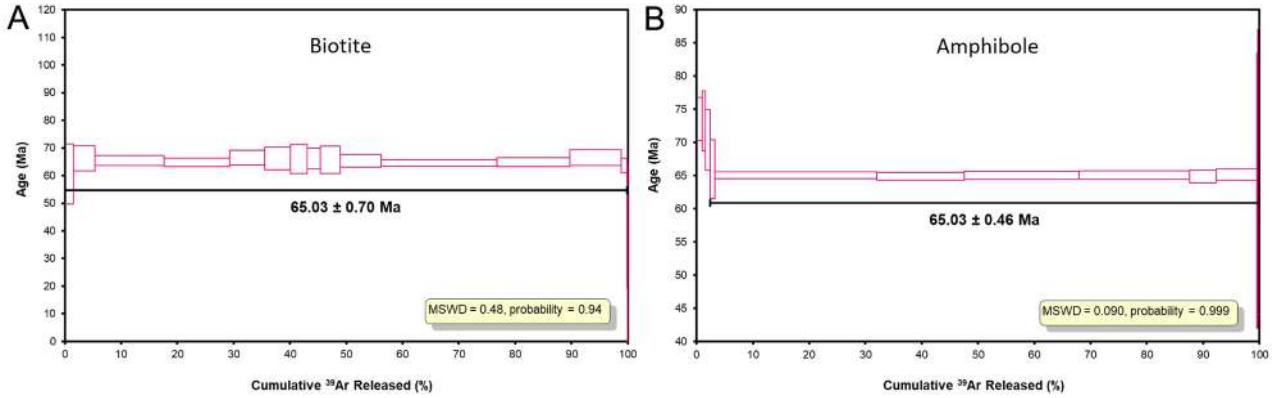

MSWD: mean squared weighted deviation.

Figure 12. ^{40}Ar-^{39}Ar step-heating dating diagrams for nepheline syenite samples of Rio Bonito complex, State of Rio de Janeiro, Brazil: (A) biotite of the sample RIB01-B; (B) amphibole of the sample RIB01-A.

with MSWD = 0.49 and probability 48% according to the Figure 13A. The selected spots have discordance of 0% and only one point that have 4% discordance (see Appendix 1). The sample RB-02 shows a concordant age of 65.18 ± 0.6 Ma with MSWD = 0.013 and probability of 91% according to the Figure 13B. The selected spots have discordance of between 0% (see Appendix 2).

Twenty-four and twenty Lu-Hf analyses were made for the samples RB-01 and RB-02 respectively. Sample RB-01 exhibits variable initial $^{176}Hf/^{177}Hf$ ratios from 0.282102 to 0.282586 (Figure 14A) and ε_{Hf} values ranging from -5.6 to -25.7 (Figure 14B) with T_{DM} values between 1.1 and 2.4 Ga (see Appendix 3). Sample RB-02 exhibits variable initial $^{176}Hf/^{177}Hf$ ratios from 0.281816 to 0.282559 (Figure 14C) and ε_{Hf} ranging from -6.5 to -33.2 (Figure 14D) with T_{DM} values between 1.2 and 2.8 Ga (see Appendix 4).

DISCUSSION

Silica undersaturated magmas cannot evolve to silica oversaturated ones by fractional crystallization, and crustal assimilation is evoked to explain this phenomenon (Sichel et al., 2012). The continental crust assimilation transforms SiO_2-undersaturated original nepheline syenite magma into SiO_2-oversaturated alkali feldspar syenite magma, crossing over the thermal divide between nepheline and quartz. The SSI as originally proposed represents the grade of the crust assimilation (Motoki et al., 2010). The rocks with negative SSI are SiO_2-undersaturated and have Norm nepheline. Almost all of the felsic rocks with positive SSI, especially alkali feldspar syenite, are SiO_2-oversaturated.

In addition to the nepheline-quartz incompatibility, there is another thermodynamic incompatibility. It is based on alkali-alumina saturation. The rocks with Na + K > Al mol. are classified as peralkaline. They can crystallise alkaline clinopyroxene and alkaline amphibole, such as aegirine, aegirine-augite, riebeckite, and barkevikite. On the other hand, highly alumina-rich rocks with Na + K + 1/2Ca < Al mol. are classified as peraluminous. They can crystallise muscovite. Most of the igneous rocks have Al/Na + K > 1 and Na + K + 1/2Ca > Al, being classified as meta-aluminous. Peralkaline magmas cannot transform into peraluminous ones by fractional crystallisation (Motoki et al., 2010). It is similar to the relation between SiO_2-undersaturated and oversaturated magmas.

The Figure 15A shows that the alkaline rocks of Rio Bonito constitute a continuous trend from SiO_2-undersaturated to oversaturated compositions and from peralkaline to peraluminous one, crossing over the above-mentioned two thermodynamic incompatibilities. This phenomenon can be explained by the crustal assimilation. The fractional crystallisation trend is of the same direction and the opposite sense. Figure 15B shows that fractional crystallisation of the felsic alkaline magmas decreases either SSI and $K_2O/(K_2O + Na_2O)$, forming a positive correlation trend. On the other hand, the continental crust assimilation increases SSI, showing vertical trends.

Because of the continental crust assimilation effects, the trachytic rocks of Rio Bonito and Tanguá massifs have

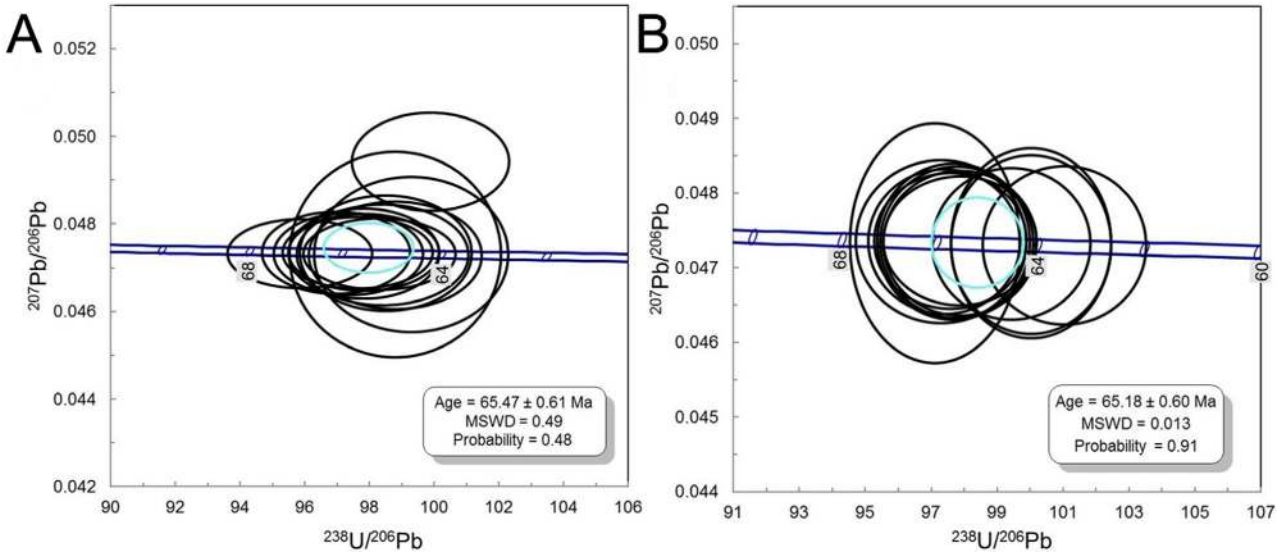

MSWD: mean squared weighted deviation.

Figure 13. U-Pb LA-ICP-MS dating diagrams for nepheline syenite samples of the Rio Bonito Complex. (A) Concordia diagram constructed with 13 analyses from the sample RB-01; (B) Concordia diagram constructed with 12 analyses from the sample RB-02.

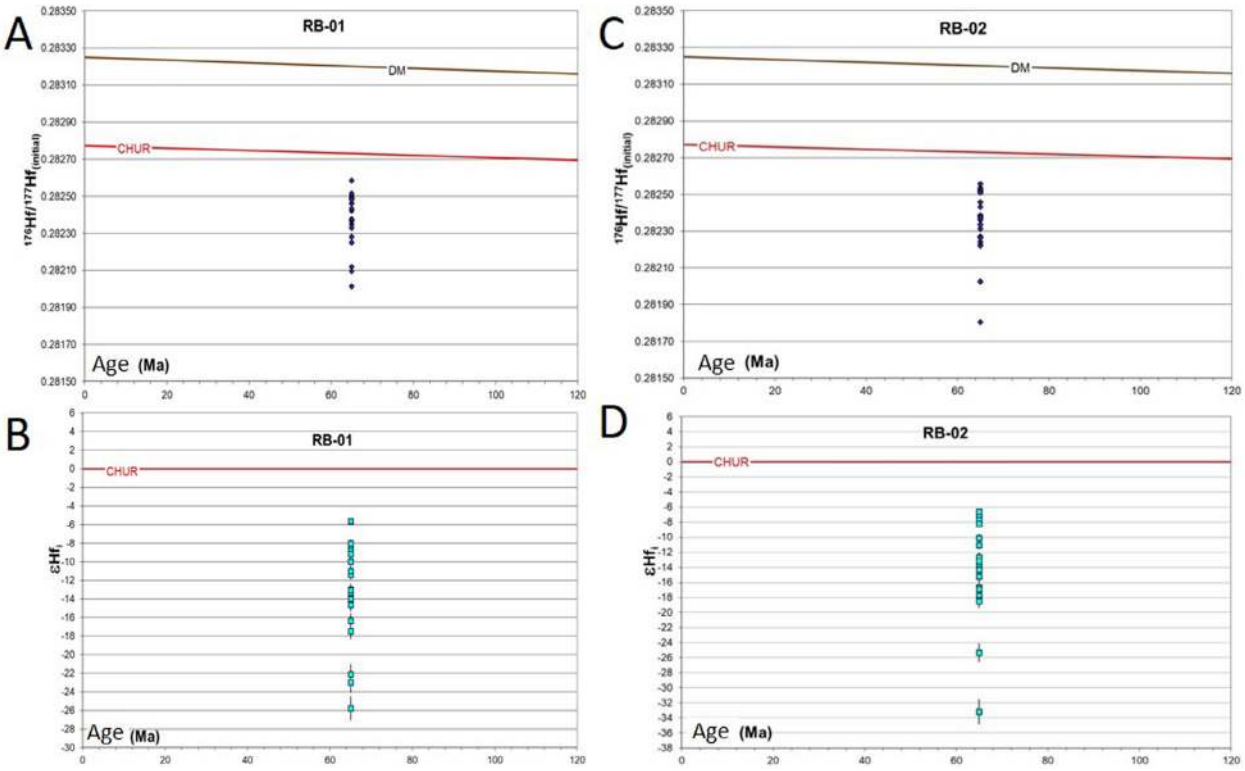

Figure 14. (A) Diagram $^{176}Hf/^{177}Hf$ vs age for 24 analyses from sample RB-01; (B) diagram ε_{Hf} vs age for 24 analyses from sample RB-01; (C) diagram $^{176}Hf/^{177}Hf$ vs age for 20 analyses from sample RB-02; (D) diagram ε_{Hf} vs age for 20 analyses from sample RB-02.

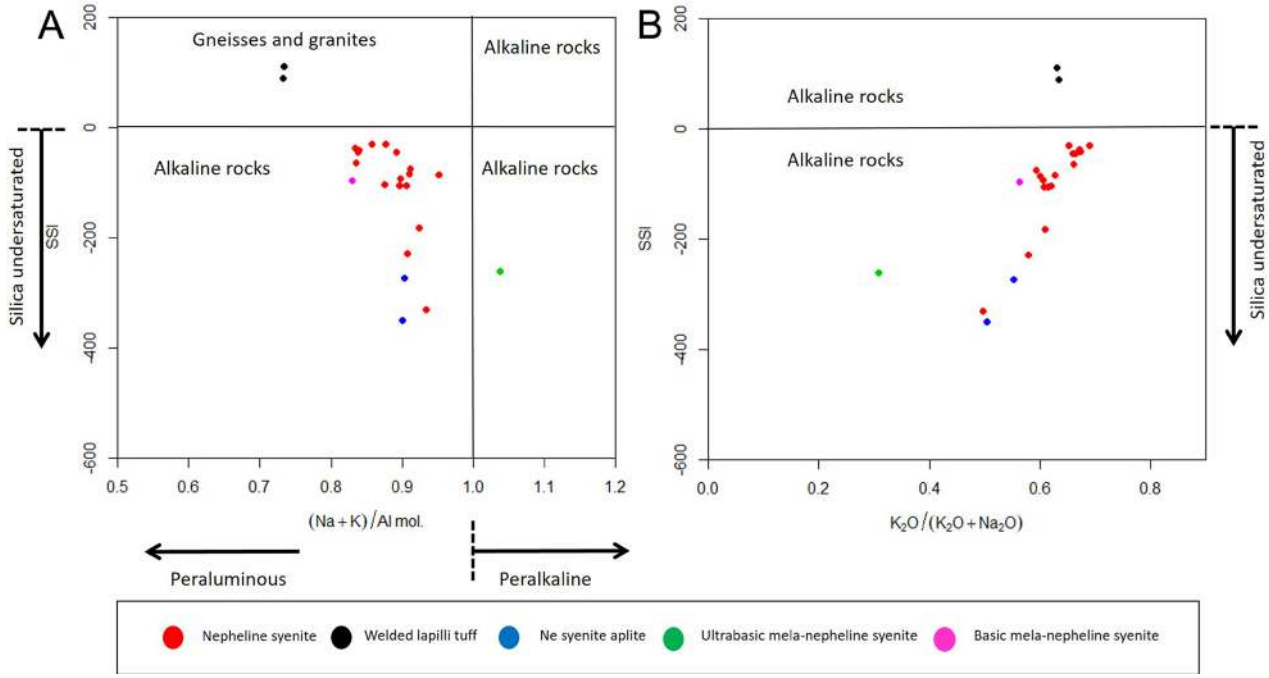

Figure 15. Variation diagrams related to the Silica Saturation Index (SSI). (A) (Na + K)/Al mol. vs. SSI; (B) $K_2O/(K_2O + Na_2O)$ vs. SSI.

normative quartz of 8.28, 6.70, 5.58, and 4.48 wt%. The alkali feldspar syenites of Tanguá and Cabo Frio Island have minor amount of normative quartz, 0.23 and 0.83 wt%. The felsic rocks of Soarinho massif have normative quartz. They plot on the area of non-alkaline rocks due to strong effects of continental crust assimilation. Among them, trachytic rocks have normative corundum.

Primary alkaline magmas are derived, in general, from water deficiency and Low-degree partial melting of an upper mantle source (McKenzie and Bickle, 1988). Bonin (1990) stated that during magma ascend and solidification, water content from wall rocks and/or after fractional crystallization may play an important role in the melt changing its composition moving from under-saturated to over-saturated alkaline melts.

The continuous geochemical trends between incompatible compositions can be formed by magma super-reheating (Motoki et al., 2010, 2013; Sichel et al., 2012). The superreheated nepheline syenite magma melts the country rock generating SiO_2-oversaturated magma. Because of the hyper-liquidus temperature, the SiO_2-undersaturated and oversaturated liquids can mix generating thermodynamically unstable alkali feldspar syenite magma. If the country rock melting is only partial, the SiO_2-oversaturated liquid should be pegmatitic with peraluminous composition. The volatile components extracted from the country rocks decrease the liquidus temperature, which makes easier the mixture between the liquids with incompatible compositions.

The nepheline syenite aplite has low total REEs, concave REE pattern, and positive Eu anomaly. These observations indicate that the aplite magma is not derived directly form the nepheline syenite magma of the main intrusive body. In addition, this rock has no cumulative plagioclase, and therefore, pointing to a reducing environment.

The large range of negative epsilon Hf can elucidate a crustal provenance for this alkaline massif contrasting with previous work based on a mantle plume origin (Thompson et al., 1998 and references therein). Both analyzed samples (RB-01 and RB-02) of Rio Bonito massif have large variation in initial $^{176}Hf/^{177}Hf$ ratios (see figures above). Griffin et al. (2002) and Andersen et al. (2002) pointed that intra sample isotopic range more likely reflects Hf isotope variations in the magma during igneous zircon growth. According to Ketchum et al. (2008), such variation is due to one or more processes that can occur in the magma source region or magma chamber. Zircon crystallization during magma mixing episodes can yield both inter- and intragrain variations in Hf isotope composition. Magma interaction with isotopically dissimilar wall rocks may also generate isotopic heterogeneity during zircon crystallization (Ketchum et al., 2008). A wide spread of $\varepsilon_{Hf(t)}$ within a single zircon crystal or among zircons from a single rock sample or thin section may result from magma mixing or contamination (Griffin et al., 2002; Kemp et al., 2007; Shaw and Flood, 2009) or indicate preservation of source heterogeneity (Farina et al., 2014).

Published Sr and Nd initial isotopic ratios (Gibson et al., 1995, 1997; Thompson et al., 1998; Ulbrich et al., 2003, 2005) point to a lithospheric mantle source for the southeastern Brazil alkaline rocks. On the other hand, our data show a set of strongly negative (-6 to -33) ε_{Hf}, indicating a possible crustal source corroborated by the SSI. Thus, the SSI could indicate not only crustal assimilation but also crustal genesis. The large variations in $^{176}Hf/^{177}Hf$ ratio showed by the Rio Bonito samples indicate zircons crystallizing from a magma undergoing assimilation of older crust, which is corroborated by trace element ratios (Rb/Ba and Rb/Sr).

CONCLUSIONS

The geochemical, geochronological, and isotopic data of the alkaline rocks of Rio Bonito intrusive complex, State of Rio de Janeiro, Brazil, lead to the following conclusions:

- Most of the analysed rocks are SiO_2-undersaturated and meta-alkaline with relatively low (Na + K)/Al and $K_2O/(Na_2O + K_2O)$, being classified as potassic nepheline syenite. The magma fractionation decreases $K_2O/(Na_2O + K_2O)$, increases (Na + K)/Al, Rb/K, and Zr/TiO_2, and the residual magma becomes more SiO_2-undersaturated.
- The variation diagrams related to TiO_2, Fe_2O_3*, MgO, CaO, and P_2O_5 indicate in-situ crystallisation and fractionation of titanite, ilmenite, apatite, and clinopyroxene or amphibole. The less fractionated nepheline syenite has unexpectedly low Zr/TiO_2.
- The RRE pattern is linear with negative gradient. Nepheline syenite aplite has low total REEs and concave pattern with positive Eu anomaly.
- The ultrabasic and basic mela-nepheline syenite samples have total REEs and light REEs concentration higher than those of the felsic alkaline rocks. These observations indicate that the nepheline syenite magma is not derived directly from the alkaline ultramafic magma by fractional crystallisation.
- Normalized REE diagram indicate a strong amphibole fractionation signature based on concavity upward with retention of middle REE.
- The laser-spot step-heating $^{40}Ar/^{39}Ar$ age for biotite is 65.03 ± 0.70 Ma and that for the amphibole is 65.03 ± 0.46 Ma. The U-Pb ages (65.49 ± 0.30 and 65.18 ± 0.30 Ma) shows that the crystallization age is indistinguishable of the cooling age. Those ages are close to the whole rock Rb-Sr age of adjacent intrusive complex of Tanguá.
- Lu-Hf data from two samples of nepheline syenite shows average ε_{Hf} values of -7 to -33, indicating that there is an

important crustal contribution to the formation of nepheline syenite magma.

ACKNOWLEDGEMENT

The present research work has been performed under the financial support of Universidade do Estado do Rio de Janeiro (UERJ), Brazil. The chemical analyses have been performed by Acme Lab. Ltd., Ontario, Canada. The laser-spot step-heating $^{40}Ar/^{39}Ar$ datings have been performed at John de Laeter Centre, Department of Applied Geology, Curtin University, Perth, Australia. The U-Pb and Lu-Hf analyses were carried out at Isotope Geochemistry Laboratory from Universidade Federal de Ouro Preto, Brazil. A part of the fieldwork instruments, office materials, and the resources of the informatics is supported by the FAPERJ (*Fundação de Amparo à Pesquisa do Estado do Rio de Janeiro, Carlos Chagas Filho*) of the State of Rio de Janeiro. This study was financed in part by the *Coordenação de Aperfeiçoamento de Pessoal de Nível Superior – Brasil* (CAPES). The authors are grateful to the above-mentioned institutions. We thank Professor Akihisa Motoki for all knowledge shared to our Institution and for the friendship throughout the years.

REFERENCES

Andersen, T., Griffin, W. L., Pearson, N. J. (2002). Crustal evolution in the SW part of the Baltic Shield: The Hf isotope evidence. *Journal of Petrology*, 43(9), 1725-1747. https://doi.org/10.1093/petrology/43.9.1725

Bataille, C. P., Willis, A., Yang, X., Liu, X. (2017). Continental igneous rock composition: A major control of past global chemical weathering. *Science Advances*, 3(3), e1602183. https://doi.org/10.1126/sciadv.1602183

Bonin, B. (1990). From orogenic to anorogenic settings: evolution of granitoid suites after a major orogenesis. *Geological Journal*, 25(3-4), 261-270. https://doi.org/10.1002/gj.3350250309

Boynton, W. V. (1984). Cosmochemistry of the rare-earth elements: meteorite studies. In: P. Henderson. *Rare-Earth Elements Geochemistry* (p. 63-114). Amsterdam: Elsevier.

Brotzu, P., Beccaluva, L., Conte, A., Fonseca, M., Garbarino, C., Gomes, C. B., Leong, R., Macciotta, G., Mansur, R. L., Melluso, L., Morbidelli, L., Ruberti, E., Sigolo, J. B., Traversa, G., Valença, J. G. (1989). Petrological and geochemical studies of alkaline rocks from continental Brazil. The syenitic intrusion of Morro Redondo, RJ. *Geochimica Brasiliensis*, 3(1), 63-80. https://doi.org/10.21715/gb.v1i3.25

Brotzu, P., Gomes, C. B., Melluso, L., Morbidelli, L., Morra, V., Ruberti, E. (1997). Petrogenesis of coexisting SiO_2-undersaturated to SiO_2-oversaturated felsic igneous rocks: the alkaline complex of Itatiaia, southern eastern Brazil. *Lithos*, 40(2-4), 133-156. https://doi.org/10.1016/S0024-4937(97)00007-8

Brotzu, P., Melluso, L., Bennio, L., Gomes, C. B., Lustrino, M., Morbidelli, L., Morra, V., Ruberti, E., Tassinari, C., D'Antonio, M. (2007). Petrogenesis of the Early Cenozoic potassic alkaline complex of Morro de São João, southeastern Brazil. *Journal of South American Earth Sciences*, 24(1), 93-115. https://doi.org/10.1016/j.jsames.2007.02.006

Dalrymple, G. B., Lanphere, M. A. (1974). $^{40}Ar/^{39}Ar$ age spectra of some undisturbed terrestrial samples. *Geochimica et Cosmochimica Acta*, 38(5), 715-738. https://doi.org/10.1016/0016-7037(74)90146-X

Farina, F., Stevens, G., Gerdes, A., Frei, D. (2014). Small-scale Hf isotopic variability in the Peninsula pluton (South Africa): the processes that control inheritance of source 176Hf/177Hf diversity in S-type granites. *Contributions to Mineralogy and Petrology*, 168, 1065. https://doi.org/10.1007/s00410-014-1065-8

Geraldes, M. C., Motoki, A., Costa, A, Mota, C. E., Mohriak, W. U. (2013a). Geochronology (Ar/Ar and K–Ar) of the South Atlantic post-break-up magmatism. *Geological Society, London, Special Publications*, 369(1), 41-74. https://doi.org/10.1144/SP369.21

Geraldes, M. C., Motoki, A., Vargas, T., Iwanuch, W., Balmant, A., Motoki, K. F. (2013b). Geology, petrography and emplacement mode of the Morro dos Gatos alkaline complex, State of Rio de Janeiro, Brazil. *Geociências*, 32(4), 625-639. Available at: <http://www.periodicos.rc.biblioteca.unesp.br/index.php/geociencias/article/view/8495>. Accessed on: Sept. 23, 2020.

Gibson, S. A., Thompson, R. N., Leonardos, O. H., Dickin, A. P., Mitchel, J. G. (1995). The late cretaceous impact of the Trindade Mantle Plume: Evidence from large-volume, mafic, potassic magmatism in SE Brazil. *Journal of Petrology*, 36(1), 189-229. https://doi.org/10.1093/petrology/36.1.189

Gibson, S. A., Thompson, R. N., Weska, R. K., Dickin, A. P., Leonardos, O. H. (1997). Late Cretaceous rift-related upwelling and melting of the Trinidade starting mantle plume head beneath western Brazil. *Contributions to Mineralogy and Petrology*, 126, 303-314. https://doi.org/10.1007/s004100050252

Griffin, W. L., Wang, X., Jackson, S. E., Pearson, N. J., O'Reilly, S. Y., Xu, X., Zhou, X. (2002). Zircon chemistry and magma mixing, SE China: *In-situ* analysis of Hf isotopes, Pingtan and Tonglu igneous complexes. *Lithos*, 61(3-4), 237-269. https://doi.org/10.1016/S0024-4937(02)00082-8

Heilbron, M., Eirado, L. G., Almeida, J. (eds.). (2016). *Mapa geológico e de recursos minerais do Estado do Rio de Janeiro*. Escala 1:400.000. Programa Geologia do Brasil (PGB). Mapas Geológicos Estaduais. Belo Horizonte: CPRM-Serviço Geológico do Brasil, Superintendência Regional de Belo Horizonte.

Heilbron, M., Machado, N. (2003). Timing of terrane accretion in the Neoproterozoic-Eopaleozoic Ribeira orogen (SE Brazil). *Precambrian Research*, 125(1-2), 87-112. https://doi.org/10.1016/S0301-9268(03)00082-2

Irvine, T. N., Baragar, W. R. A. (1971). A guide to the chemical classification of the common volcanic rocks. *Canadian Journal of Earth Sciences*, 8(5), 523-548. https://doi.org/10.1139/e71-055

Kemp, A. I. S., Hawkesworth, C. J., Foster, G. L., Paterson, B. A., Woodhead, J. D., Hergt, J. M., Gray, C. M., Whitehouse, M. J. (2007). Magmatic and crustal differentiation history of granitic rocks from hafnium and oxygen isotopes in zircon. *Science*, 315(5814), 980-983. https://doi.org/10.1126/science.1136154

Ketchum, J. W. F., Ayer, J. A., Breemen, O. V., Pearson, N. J., Becker, J. (2008). Pericontinental Crustal Growth of the Southwestern Abitibi Subprovince, Canada - U-Pb, Hf and Nd Isotope Evidence. *Economic Geology*, 103(6), 1151-1184. https://doi.org/10.2113/gsecongeo.103.6.1151

Le Bas, M. J., Le Maitre, R. W., Streckeisen, A., Zanettin, B. (1986). A Chemical Classification of Volcanic. Rocks based on the Total-Alkali-Silica Diagram. *Journal of Petrology*, 27(3), 745-750. https://doi.org/10.1093/petrology/27.3.745

Le Maitre, R. W. (2002). *Igneous Rocks:* A Classification and Glossary of Terms. 2ª ed. Cambridge: Cambridge University Press, 252 p. https://doi.org/10.1017/CBO9780511535581

Ludwig, K. R. (2003). *Using Isoplot/Ex, Version 3.00:* a Geochronological Toolkit for Microsoft Excel. Berkeley: Berkeley Geochronology Center, Special Publication, v. 4, 74 p.

Maniar, P. D., Piccoli, P. M. (1989). Tectonic discrimination of granitoids. *Geological Society of America Bulletin*, 101(5), 635-643. https://doi.org/10.1130/0016-7606(1989)101<0635:TDOG>2.3.CO;2

McKenzie, D. P., Bickle, M. J. (1988). The volume and composition of melt generated by extension of the lithosphere. *Journal of Petrology*, 29(3), 625-679. https://doi.org/10.1093/petrology/29.3.625

Middlemost, E. A. K. (1975). The basalt clan. *Earth Science Reviews*, 11, 337-364. https://doi.org/10.1016/0012-8252(75)90039-2

Mota, C. E. M., Geraldes, M. C. (2006). A classificação de brechas magmáticas e sua implicação na evolução do Complexo Alcalino de Nova Iguaçu–RJ. *Geociências*, 25(1), 37-48. Available at: <http://www.periodicos.rc.biblioteca.unesp.br/index.php/geociencias/article/view/121>. Accessed on: Sept. 23, 2020.

Mota, C. E. M., Geraldes, M. C., Almeida, J. C. H., Vargas, T., Souza, D. M., Loureiro, R. O., Silva, A. P. (2009). Características Isotópicas (Nd e Sr), Geoquímicas e Petrográficas da Intrusão Alcalina do Morro de São João: Implicações Geodinâmicas e Sobre a Composição do Manto Sublitosférico. *Geologia USP. Série Científica*, 9(1), 85-100. https://doi.org/10.5327/Z1519-874X2009000100006

Motoki, A., Araújo, A. L., Sichel, S. E., Geraldes, M. C., Jourdan, F., Motoki, K. F., Silva, S. (2013). Nepheline syenite magma differentiation process by continental crustal assimilation for the Cabo Frio Island intrusive complex, State of Rio de Janeiro, Brazil. *Geociências*, 32(2), 195-218. Available at: <http://www.periodicos.rc.biblioteca.unesp.br/index.php/geociencias/article/view/8329>. Accessed on: Sept. 23, 2020.

Motoki, A., Geraldes, M. C., Iwanuch, W., Vargas, T., Motoki, K. F., Balmant, A., Ramos, M. N. (2012a). Pyroclastic dyke and welded crystal tuff of the Morro dos Gatos alkaline intrusive complex, State of Rio de Janeiro, Brazil. *REM: Revista Escola de Minas*, 65(1), 35-45. https://doi.org/10.1590/S0370-44672012000100006

Motoki, A., Sichel, S. E. (2006). Avaliação de aspectos texturais e estruturais de corpos vulcânicos e subvulcânicos e sua relação com o ambiente de cristalização, com base em exemplos do Brasil, Argentina e Chile. *REM: Revista Escola de Minas*, 59(1), 13-23. https://doi.org/10.1590/S0370-44672006000100003

Motoki, A., Sichel, S. E. (2008). Hydraulic fracturing as possible mechanism of dyke-sill transition and horizontal discordant intrusion: an example of Arraial do Cabo area, State of Rio de Janeiro, Brazil. *Geofísica Internacional*, 47(1), 3-25. Available at: <http://www.scielo.org.mx/scielo.php?script=sci_arttext&pid=S0016-71692008000100002>. Accessed on: Sept. 23, 2020.

Motoki, A., Sichel, S. E., Petrakis, G. H. (2009). Genesis of the tabular xenoliths along contact plane of the mafic dykes of Cabo Frio area, state of Rio de Janeiro, Brazil: Thermal delamination or hydraulic shear fracturing? *Geociências*, 28(1), 15-26. Available at: <http://www.periodicos.rc.biblioteca.unesp.br/index.php/geociencias/article/view/3416>. Accessed on: Sept. 23, 2020.

Motoki, A., Sichel, S. E., Savi, D. C., Aires, J. R. (2008a). Intrusion mechanism of tabular intrusive bodies of subhorizontal discordant emplacement of the Cabo Frio Islands and the neighbor areas, State of Rio de Janeiro, Brazil. *Geociências*, 27(2), 207-218. Available at: <http://www.periodicos.rc.biblioteca.unesp.br/index.php/geociencias/article/view/3407>. Accessed on: Sept. 23, 2020.

Motoki, A., Sichel, S. E., Soares, R. S., Aires, J. R., Savi, D. C., Petrakis, G. H., Motoki, K. F. (2008b). Vent-filling pyroclastic rocks of the Mendanha, the Itaúna, and the Cabo Frio Island, State of Rio de Janeiro, Brazil, and their formation process based of the conduit implosion model. *Geociências*, 27(4), 451-467. Available at: <http://www.periodicos.rc.biblioteca.unesp.br/index.php/geociencias/article/view/3415>. Accessed on: Sept. 23, 2020.

Motoki, A., Sichel, S. E., Soares, R. S., Neves, J. L. P., Aires, J. R. (2008c). Geological, lithological, and petrographical characteristics of the Itaúna Alkaline Intrusive Complex, São Gonçalo, State of Rio de Janeiro, Brazil, with special attention of its emplace mode. *Geociências*, 27(1), 33-44. Available at: <http://www.periodicos.rc.biblioteca.unesp.br/index.php/geociencias/article/view/3394>. Accessed on: Sept. 23, 2020.

Motoki, A., Sichel, S. E., Vargas, T., Aires, J. R., Iwanuch, W., Melo, S. L. M., Motoki, K. F., Silva, S., Balmant, A. (2010). Geochemical evolution of the felsic alkaline rocks of Tanguá, Rio Bonito, and Itaúna intrusive bodies, State of Rio de Janeiro, Brazil. *Geociências*, 29(3), 291-310. Available at: <http://www.periodicos.rc.biblioteca.unesp.br/index.php/geociencias/article/view/5384>. Accessed on: Sept. 23, 2020.

Motoki, A., Soares, R., Netto, A. M., Sichel, S. E., Aires, J. R., Lobato, M. (2007a). Geologic occurrence shape of pyroclastic rock dykes in the Dona Eugênia River Valley, Municipal Park of Nova Iguaçu, Rio de Janeiro. *Geociências*, 26(1), 67-82. Available at: <http://www.periodicos.rc.biblioteca.unesp.br/index.php/geociencias/article/view/1707>. Accessed on: Sept. 23, 2020.

Motoki, A., Soares, R., Netto, A. M., Sichel, S. E., Aires, J. R., Lobato, M. (2007b). Genetic reconsideration of the Nova Iguaçu Volcano model, State of Rio de Janeiro, Brazil: eruptive origin or subvolcanic intrusion? *REM: Revista Escola de Minas*, 60(4), 583-592. https://doi.org/10.1590/S0370-44672007000400003

Motoki, A., Soares, R., Sichel, S. E., Aires, J. R., Lobato, M. (2007c). Weathering fabrics in felsic alkaline rocks of Nova Iguaçu, State of Rio de Janeiro, Brazil. *REM: Revista Escola de Minas*, 60(3), 451-458. https://doi.org/10.1590/S0370-44672007000300003

Motoki, A., Vargas, T., Iwanuch, W., Melo, D. P., Sichel, S. E., Balmant, A., Aires, J. R., Motoki, K. F. (2012b). Fossil earthquake evidenced by the silicified tectonic breccia of the Cabo Frio area, State of Rio de Janeiro, Brazil, and its bearings on the genesis of stick-slip fault movement and the associated amagmatic hydrothermalism. *Anuário do Instituto de Geociências*, 35(2), 124-139. https://doi.org/10.11137/2012_2_124_139

Motoki, A., Vargas, T., Iwanuch, W., Sichel, S. E., Balmant, A., Aires, J. R. (2011). Tectonic breccia of the Cabo Frio area, State of Rio de Janeiro, Brazil, intruded by Early Cretaceous mafic dyke: evidence of the Pan-African brittle tectonism? *REM: Revista Escola de Minas*, 64(1), 25-36. https://doi.org/10.1590/S0370-44672011000100003

Sadowski, G. R., Dias Neto, C. M. (1981). O lineamento sismotectônico de Cabo Frio. *Revista Brasileira de Geociências*, 11(4), 209-212. https://doi.org/10.25249/0375-7536.1981209212

Schmitt, R. S., Trouw, R. A. J., Van Schmus, W. R., Pimentel, A. M. (2004). Late amalgamation in the central part of West Gondwana: new geochronological data and the characterization of a Cambrian collisional orogeny in the Ribeira Belt (SE Brazil). *Precambrian Research*, 133(1-2), 29-61. https://doi.org/10.1016/j.precamres.2004.03.010

Shaw, S. E., Flood., R. H. (2009). Zircon Hf Isotopic Evidence for Mixing of Crustal and Silicic Mantle-derived Magmas in a Zoned Granite Pluton, Eastern Australia. *Journal of Petrology*, 50(1), 147-168. https://doi.org/10.1093/petrology/egn078

Sichel, S. E., Motoki, A., Iwanuch, W., Vargas, T., Aires, J. R., Melo, D. P., Motoki, K. F., Balmant, A., Rodrigues, J. G. (2012). Fractionation crystallisation and continental crust assimilation by the felsic alkaline rock magmas of the State of Rio de Janeiro, Brazil. *Anuário do Instituto de Geociências*, 35(2), 84-104. http://doi.org/10.11137/2012_2_84_104

Sichel, S. E., Motoki, A., Savi, D. C., Soares, R. S. (2008). Subvolcanic vent-filling welded tuff breccia of the Cabo Frio Island, State of Rio de Janeiro, Brazil. *REM: Revista Escola de Minas*, 61(4), 423-432. https://doi.org/10.1590/S0370-44672008000400004

Silva, D. A., Geraldes, M. C., Vargas, T., Jourdan, F., Nogueira, C. C. (2015). $^{40}Ar/^{39}Ar$ age, lithogeochemistry and petrographic studies of the Cretaceous Alkaline Marapicu Intrusion, Rio de Janeiro, Brazil. *Boletim do Museu Paraense Emílio Goeldi. Ciências Naturais*, 10(3), 399-422. Available at: <http://editora.museu-goeldi.br/bn/artigos/cnv10n3_2015/40(silva).pdf>. Accessed on: Sept. 23, 2020.

Stewart, K., Turner, S., Kelley, S., Hawkesworth, C., Kirstein, L., Mantovani, M. (1996). 3-D, Ar-Ar geochronology in the Paraná continental flood basalt province. *Earth and Planetary Science Letters*, 143(1-4), 95-109. https://doi.org/10.1016/0012-821X(96)00132-X

Sun, S., McDonough, W. F. (1989). Chemical and isotopic systematics of oceanic basalts: Implications for mantle composition and processes. In: A. D. Saunders, M. J. Norry (eds). *Magmatism in the ocean basins* (p. 313-345). Boston: Blackwell Scientific.

Tera, F., Wasserburg, G. J. (1972). U-Th-Pb systematic in three Apolo 14 basalts and the problem of initial Pb in lunar rocks. *Earth and Planetary Science Letters*, 14(3), 281-304. https://doi.org/10.1016/0012-821X(72)90128-8

Thompson, R. N., Gibson, S. A., Mitchell, J. G., Dickin, A. P., Leonardos, O. H., Brod, J. A., Greenwood, J. C. (1998). Migrating Cretaceous–Eocene Magmatism in the Serra do Mar Alkaline Province, SE Brazil: Melts from the Deflected Trindade Mantle Plume? *Journal of Petrology*, 39(8), 1493-1526. https://doi.org/10.1093/petroj/39.8.1493

Thornton, C. P., Tuttle, O. F. (1960). Chemistry of igneous rocks, part I. Differentiation index. *American Journal of Science*, 258(9), 664-684. https://doi.org/10.2475/ajs.258.9.664

Ulbrich, H. H., Demaiffe, D., Vlach, S. R. F., Ulbrich, M. N. C. (2003). Geochemical and Sr, Nd, and Pb isotope signatures of phonolites and nepheline syenites from the Poços de Caldas Alkaline Massif, southeastern Brazil. *IV South American Symposium on Isotope Geology*. Salvador, p. 698-701.

Ulbrich, H. H., Vlach, S. R. F., Demaiffe, D., Ulbrich, M. N. C. 2005. Structure and origin of the Poços de Caldas Alkaline Massif. In: P. Comin-Chiaramonti, C. B. Gomes (eds.). *Mesozoic to Cenozoic Alkaline Magmatism in the Brazilian Platform* (p. 367-418). São Paulo: Edusp/Fapesp.

Valeriano, C. M., Tupinambá, M., Simonetti, A., Heilbron, M., Almeida, J. C. H., Eirado, L. G. (2011). U-Pb LA-MC-ICPMS geochronology of Cambro-Ordovician post-collisional granites of the Ribeira belt, southeast Brazil: Terminal Brasiliano magmatism in central Gondwana supercontinent. *Journal of South American Earth Sciences*, 32(4), 416-428. https://doi.org/10.1016/j.jsames.2011.03.003

Wendt, I., Carl, C. (1991). The statistical distribution of the mean squared weighted deviation. *Chemical Geology: Isotope Geoscience Section*, 86(4), 275-285. https://doi.org/10.1016/0168-9622(91)90010-T

Appendix 1. U-Pb data of 28 analyses from the sample RB-01.

Spot	f206	^{207}Pb	^{206}Pb	U	Th/U	^{207}Pb/ ^{206}Pb	2 s (%)	^{207}Pb/ ^{235}U	2 s (%)	^{206}Pb/ ^{238}U	2 s (%)	Rho	^{207}Pb/ ^{206}Pb	2 s	^{206}Pb/ ^{238}U	2 s	^{207}Pb/ ^{235}U	2 s	% conc
7	0,1723	244,022	11,525	1011	0,75	0,04722849	1,30	0,069706341	3,79	0,010704514	3,56	0,94	61	31,05	69	2,42	68	2,50	100
8	0,8516	124,819	5,856	543	0,57	0,046917016	4,05	0,065998658	17,34	0,010202426	16,86	0,97	45	96,74	65	10,94	65	10,91	101
9	0	22,033	1,042	97	0,98	0,0473	3,28	0,066013489	3,94	0,010122092	2,18	0,55	64	78,03	65	1,40	65	2,47	100
10	1	159,985	7,600	670	0,68	0,04750387	4,36	0,069389293	19,51	0,010594054	19,02	0,97	75	103,65	68	12,81	68	12,89	100
11	0,2643	290,787	13,727	1250	0,56	0,047204909	1,56	0,067187936	5,59	0,010322927	5,37	0,96	60	37,09	66	3,52	66	3,57	100
12	0	107,956	5,111	464	0,62	0,04734	1,31	0,067314669	2,04	0,010312885	1,56	0,77	66	31,18	66	1,02	66	1,30	100
13	1	153,620	7,285	652	1,83	0,047420077	4,43	0,068347715	19,78	0,01045347	19,27	0,97	70	105,49	67	12,81	67	12,88	100
14	0	106,784	5,049	468	0,44	0,04728	1,71	0,065985577	2,47	0,010122092	1,79	0,72	63	40,80	65	1,15	65	1,55	100
15	0	227,234	10,753	966	1,44	0,04732	1,10	0,068072437	1,89	0,010433386	1,54	0,81	65	26,16	67	1,02	67	1,22	100
16	0	62,408	2,951	272	0,59	0,04729	1,61	0,066261436	2,40	0,010162259	1,78	0,74	64	38,27	65	1,15	65	1,51	100
17	0	81,140	3,839	350	0,36	0,04731	1,31	0,067009997	2,04	0,010272718	1,56	0,77	65	31,20	66	1,02	66	1,30	100
18	1	101,181	4,796	442	0,61	0,047398616	4,42	0,066348	20,33	0,010152217	19,85	0,98	69	105,25	65	12,82	65	12,88	100
19	0	51,421	2,541	228	0,63	0,04942	1,50	0,06821956	2,19	0,010011633	1,60	0,73	168	34,98	64	1,02	67	1,42	96
20	0	74,529	3,527	323	0,51	0,04732	1,44	0,066696575	2,13	0,010222509	1,57	0,74	65	34,21	66	1,02	66	1,35	100
27	0,8335	41,061	1,927	181	0,43	0,046935524	4,30	0,064984934	17,33	0,010041758	16,79	0,97	46	102,81	64	10,72	64	10,75	101
28	0,5223	190,109	8,951	824	1,8	0,047082817	2,53	0,066492648	10,66	0,010242593	10,36	0,97	53	60,31	66	6,75	65	6,75	100
29	1,0588	145,851	6,839	642	1,19	0,046888227	4,90	0,065179127	21,73	0,010081925	21,17	0,97	44	117,12	65	13,58	64	13,54	101
30	4,3958	54,446	2,462	239	1,82	~~0,045211233~~	~~19,53~~	~~0,062910542~~	~~89,65~~	~~0,010091967~~	~~87,49~~	~~0,98~~	~~-44~~	~~474,65~~	~~65~~	~~56,37~~	~~62~~	~~55,13~~	~~104~~
31	0	40,836	1,932	180	1,08	0,0473	2,47	0,065686042	3,18	0,010071883	1,99	0,63	64	58,90	65	1,28	65	1,98	100
32	0,4719	162,776	7,699	630	1,04	0,047295775	2,35	0,074716928	8,74	0,011457646	8,42	0,96	64	56,04	73	6,13	73	6,17	100
33	0,1182	145,033	6,852	633	0,59	0,047244079	1,29	0,066262505	3,10	0,010172301	2,82	0,91	62	30,66	65	1,82	65	1,95	100
34	0,3496	203,810	9,609	895	0,26	0,047144588	2,04	0,065666043	7,42	0,010102008	7,13	0,96	57	48,64	65	4,58	65	4,63	100
35	0	111,799	5,294	485	0,98	0,04735	1,22	0,066738859	1,99	0,010222509	1,57	0,79	67	29,16	66	1,02	66	1,26	100
36	0	155,449	7,354	678	0,98	0,04731	1,14	0,066354963	1,95	0,010172301	1,58	0,81	65	27,18	65	1,02	65	1,23	100
37	0	157,705	7,466	683	0,36	0,04734	1,14	0,066855854	1,94	0,010242593	1,57	0,81	66	27,15	66	1,02	66	1,23	100
38	0	67,939	3,216	297	1,91	0,04733	1,84	0,066251952	2,56	0,010152217	1,78	0,70	66	43,76	65	1,15	65	1,61	100
39	0,2266	82,632	3,902	360	0,23	0,047222747	1,98	0,066363351	5,20	0,010192384	4,80	0,92	61	47,28	65	3,11	65	3,28	100
40	1,882	113,837	5,290	496	1,38	~~0,046468706~~	~~8,27~~	~~0,065303678~~	~~38,03~~	~~0,010192384~~	~~37,12~~	~~0,98~~	~~22~~	~~198,56~~	~~65~~	~~24,09~~	~~64~~	~~23,85~~	~~102~~

Appendix 2. U-Pb data of 28 analyses from the sample RB-02.

Spot	f206	^{207}Pb	^{206}Pb	U	Th/U	$^{207}Pb/^{206}Pb$	2 s (%)	$^{207}Pb/^{235}U$	2 s (%)	$^{206}Pb/^{238}U$	2 s (%)	Rho	$^{207}Pb/^{206}Pb$	2 s	$^{206}Pb/^{238}U$	2 s	$^{207}Pb/^{235}U$	2 s	% conc
47	1,8508	18,579	863	80	0,94	0,046473623	8,71	0,067397389	36,38	0,010518051	35,32	0,97	22	209,11	67	23,70	66	23,55	102
48	0	47,425	2,592	206	1,48	~~0,05465~~	~~2,36~~	~~0,07880212~~	~~3,04~~	~~0,010457948~~	~~1,92~~	~~0,63~~	~~398~~	~~52,91~~	~~67~~	~~1,28~~	~~77~~	~~2,25~~	~~87~~
49	0	69,814	3,305	309	2,31	0,04734	1,42	0,06675768	2,11	0,010227552	1,57	0,74	66	33,69	66	1,02	66	1,34	100
50	0	35,359	1,674	160	1,6	0,04733	1,77	0,06524005	2,39	0,009997157	1,60	0,67	66	42,25	64	1,02	64	1,49	100
51	0	66,555	3,149	302	2,53	0,04731	1,67	0,065212482	2,31	0,009997157	1,60	0,69	65	39,76	64	1,02	64	1,44	100
52	0	37,349	1,768	164	1,52	0,04733	2,24	0,067201174	2,84	0,010297673	1,75	0,62	66	53,32	66	1,15	66	1,82	100
53	0,4157	117,753	5,548	527	3,08	0,047113316	2,18	0,0657873	8,65	0,01012738	8,38	0,97	55	51,92	65	5,41	65	5,43	100
54	1	56,389	2,673	246	1,85	0,047395148	4,56	0,068013742	19,86	0,010407862	19,33	0,97	69	108,51	67	12,82	67	12,90	100
55	1	136,382	6,476	610	2,21	0,047484426	4,40	0,066371089	20,31	0,010137398	19,83	0,98	74	104,53	65	12,82	65	12,89	100
56	0,2593	147,266	6,961	638	3,01	0,047267102	1,65	0,068221695	5,45	0,010467965	5,19	0,95	63	39,21	67	3,46	67	3,53	100
57	0,188	65,349	3,088	292	1,96	0,04725099	1,70	0,065979544	4,39	0,01012738	4,04	0,92	62	40,51	65	2,61	65	2,76	100
58	0	60,197	2,850	265	1,9	0,04735	1,52	0,067098774	2,32	0,010277638	1,75	0,76	67	36,19	66	1,15	66	1,48	100
59	0,9236	20,125	944	91	0,99	0,046912683	4,59	0,065183172	19,01	0,010077294	18,45	0,97	45	109,79	65	11,86	64	11,86	101
60	0	95,723	4,532	423	3,62	0,04735	1,35	0,067033375	2,06	0,010267621	1,56	0,76	67	32,17	66	1,02	66	1,32	100
67	0	93,892	4,444	417	3,4	0,04733	1,35	0,066678207	2,07	0,010217535	1,57	0,76	66	32,19	66	1,02	66	1,31	100
68	0,1539	91,476	4,327	400	2,92	0,047297106	1,67	0,067677073	3,83	0,01037781	3,44	0,90	64	39,89	67	2,28	66	2,46	100
69	0	124,010	5,873	549	2,42	0,04736	1,27	0,066916708	2,01	0,010247587	1,56	0,78	67	30,15	66	1,02	66	1,28	100
70	1	121,800	5,772	537	2,6	0,047387837	4,59	0,067152392	20,10	0,010277638	19,57	0,97	69	109,31	66	12,83	66	12,91	100
71	2,2069	72,085	3,336	316	2,54	0,046285474	9,69	0,065973824	43,89	0,010337741	42,80	0,98	13	233,05	66	28,25	65	27,92	102
72	0,4917	90,269	4,251	399	2,77	0,047097257	2,50	0,066545468	10,06	0,010247587	9,74	0,97	54	59,72	66	6,36	65	6,38	100
73	0,2946	161,794	7,635	715	4,89	0,047190544	1,75	0,066742455	6,22	0,010257604	5,96	0,96	59	41,77	66	3,90	66	3,95	100
74	0	100,258	4,747	444	2,2	0,04735	1,46	0,06683718	2,14	0,010237569	1,57	0,73	67	34,68	66	1,02	66	1,36	100
75	1	40,737	1,945	185	1,43	0,047748398	4,71	0,065618927	20,72	0,009967105	20,18	0,97	87	111,72	64	12,83	65	13,02	99
76	0	187,948	8,901	834	4,84	0,04736	1,20	0,066720471	1,98	0,010217535	1,57	0,79	67	28,64	66	1,02	66	1,25	100
77	0	68,003	3,218	306	2,08	0,04732	1,42	0,065618408	2,13	0,01005726	1,59	0,75	65	33,71	65	1,02	65	1,33	100
78	1,5436	68,796	3,204	315	2,19	0,046579733	6,88	0,063626865	32,01	0,009907002	31,26	0,98	28	164,97	64	19,76	63	19,60	101
79	0	79,183	3,745	363	2,25	0,0473	1,48	0,064545404	2,19	0,009896985	1,62	0,74	64	35,24	63	1,02	64	1,35	100
80	0,3488	79,945	3,768	364	2,05	0,047134998	2,16	0,064775953	7,51	0,009967105	7,19	0,96	56	51,46	64	4,57	64	4,64	100

Appendix 3. Lu-Hf data of 23 analyses from the sample RB-01.

Spot	$^{176}Yb/^{177}Hf$	± 2s a	$^{176}Lu/^{177}Hf$	± 2s b	$^{178}Hf/^{177}Hf$	$^{180}Hf/^{177}Hf$	SigHf	$^{176}Hf/^{177}Hf$	± 2s c	$^{176}Hf/^{177}Hf(t)$	$\varepsilon_{Hf(t)}$	± 2s d	Avg MORB	TDM2 f	TDM2 g	age	± 2s e
22	0,1116	90	0,00288	18	1,46671	1,88707	6	0,282426	22	0,282422043	-11,39395	1,22168	1,4	1,7	1,4	65	0
23	0,244	210	0,00597	41	1,46669	1,88676	7	0,282102	21	0,282094551	-22,97656	2,24845	2	2,3	2	65	0
24	0,1206	144	0,00274	29	1,46671	1,88681	8	0,28238	25	0,282376223	-13,03666	1,65981	1,5	1,8	1,5	65	0
25	0,0866	87	0,00219	18	1,46669	1,88687	7	0,282436	24	0,282433095	-11,00305	1,19976	1,4	1,6	1,4	65	0
26	0,0582	47	0,00133	8	1,46671	1,88684	9	0,28251	30	0,282508308	-8,34296	0,94779	1,3	1,5	1,2	65	0
27	0,0769	63	0,00176	11	1,46663	1,88685	8	0,282464	28	0,282461597	-9,97281	1,03728	1,3	1,6	1,3	65	0
28	0,162	163	0,0039	29	1,46664	1,88683	7	0,282255	21	0,282250177	-17,47244	1,82219	1,8	2	1,7	65	0
29	0,1197	98	0,00254	17	1,46666	1,88704	8	0,282352	27	0,282349281	-13,96735	1,27626	1,6	1,8	1,5	65	0
30	0,1321	118	0,00313	21	1,46667	1,88683	6	0,282334	25	0,282329876	-14,65366	1,43728	1,6	1,8	1,6	65	0
31	0,0701	59	0,00162	11	1,46667	1,88699	7	0,282489	30	0,282486919	-9,07722	1,01416	1,3	1,5	1,3	65	0
32	0,0837	70	0,00196	12	1,46671	1,88692	8	0,282464	22	0,28246121	-10,00868	1,08136	1,3	1,6	1,3	65	0
33	0,0658	56	0,00156	10	1,46671	1,88708	7	0,282494	30	0,28249239	-8,92813	0,99771	1,3	1,5	1,3	65	0
34	0,1501	134	0,00327	21	1,46665	1,8871	9	0,282285	20	0,282281297	-16,37179	1,56775	1,7	1,9	1,7	65	0
35	0,1267	107	0,00295	18	1,46669	1,88685	7	0,282368	22	0,282364063	-13,42237	1,35257	1,5	1,8	1,5	65	0
36	0,1187	98	0,00262	18	1,46662	1,88684	8	0,282376	29	0,282372303	-13,13095	1,28041	1,5	1,8	1,5	65	0
37	0,1217	101	0,00264	18	1,4666	1,88691	8	0,28237	27	0,28236624	-13,30101	1,30542	1,5	1,8	1,5	65	0
38	0,1279	120	0,00297	20	1,46659	1,88679	7	0,282381	27	0,28237712	-13,00493	1,45135	1,5	1,8	1,5	65	0
39	0,2536	231	0,00586	48	1,46661	1,88696	8	0,282022	23	0,282014913	-25,77101	2,44777	2,2	2,4	2,2	65	0
40	0,0791	89	0,0017	16	1,46655	1,88696	9	0,282495	23	0,282493355	-8,82741	1,21327	1,3	1,5	1,3	65	0
41	0,0271	24	0,00063	4	1,46645	1,88683	7	0,282586	29	0,282585584	-5,60986	0,85845	1,1	1,4	1,1	65	0
42	0,0574	46	0,00139	8	1,46646	1,88696	8	0,282518	28	0,282516121	-8,02223	0,94497	1,2	1,5	1,2	65	0
43	0,1234	101	0,00277	17	1,46645	1,88708	9	0,282379	23	0,282375215	-13,05014	1,30355	1,5	1,8	1,5	65	0
44	0,0874	71	0,00198	12	1,46651	1,88701	8	0,282485	32	0,282482023	-9,18381	1,08831	1,3	1,6	1,3	65	0

Appendix 4. Lu-Hf data of 20 analyses from the sample RB-02.

Spot	$^{176}Yb/^{177}Hf$	± 2s a	$^{176}Lu/^{177}Hf$	± 2s b	$^{178}Hf/^{177}Hf$	$^{180}Hf/^{177}Hf$	SigHf	$^{176}Hf/^{177}Hf$	± 2s c	$^{176}Hf/^{177}Hf(t)$	$\varepsilon_{Hf(t)}$	± 2s d	Avg MORB	TDM2 f	TDM2 g	age	± 2s e
126	0,2969	239	0,00894	54	1,46695	1,88679	5	0,281816	25	0,281805346	-33,18292	2,51925	2,6	2,8	2,6	65	0
127	0,2375	261	0,00552	63	1,46685	1,88697	7	0,282033	17	0,282026521	-25,36048	2,73426	2,2	2,4	2,2	65	0
128	0,0827	67	0,0021	14	1,46679	1,88678	6	0,28246	16	0,282457171	-10,12933	1,06324	1,4	1,6	1,3	65	0
129	0,1431	117	0,00366	22	1,4668	1,88683	6	0,282319	13	0,282314227	-15,20715	1,42775	1,6	1,9	1,6	65	0
130	0,1243	108	0,0032	22	1,46689	1,88708	6	0,282384	17	0,282379584	-12,87342	1,35514	1,5	1,8	1,5	65	0
131	0,1093	91	0,00262	17	1,4668	1,88701	7	0,282436	16	0,282432603	-11,04264	1,22402	1,4	1,6	1,4	65	0
132	0,1596	141	0,00374	25	1,46686	1,88688	6	0,282276	17	0,282271298	-16,68109	1,63464	1,7	2	1,7	65	0
133	0,1749	140	0,0042	25	1,4668	1,88689	6	0,282246	15	0,282241167	-17,76891	1,6255	1,8	2	1,8	65	0
134	0,1663	133	0,00399	24	1,46672	1,88676	6	0,282271	20	0,282266234	-16,90452	1,56642	1,7	2	1,7	65	0
135	0,1098	88	0,00274	16	1,46675	1,88689	6	0,28239	18	0,282386174	-12,64035	1,20566	1,5	1,7	1,5	65	0
136	0,0573	46	0,00142	9	1,46668	1,88685	6	0,282519	21	0,28251767	-8,01183	0,94417	1,2	1,5	1,2	65	0
137	0,0574	46	0,00151	9	1,46671	1,88707	6	0,28254	21	0,282537738	-7,27989	0,94382	1,2	1,4	1,2	65	0
138	0,1345	108	0,00323	19	1,46679	1,88699	5	0,282364	21	0,282359841	-13,57169	1,35492	1,5	1,8	1,5	65	0
139	0,208	166	0,00496	30	1,46677	1,88699	6	0,282232	21	0,282226356	-18,31494	1,85483	1,8	2	1,8	65	0
140	0,0602	48	0,00155	9	1,46672	1,88681	6	0,282526	26	0,282524107	-7,73979	0,95503	1,2	1,5	1,2	65	0
141	0,0562	45	0,00133	8	1,4668	1,88678	8	0,282512	16	0,282510729	-8,23512	0,93895	1,3	1,5	1,2	65	0
142	0,1755	140	0,00429	26	1,46675	1,88684	6	0,282226	16	0,282220829	-18,48825	1,62545	1,8	2,1	1,8	65	0
143	0,1321	106	0,00313	19	1,46667	1,88683	6	0,282342	16	0,282337824	-14,35039	1,3393	1,6	1,8	1,6	65	0
144	0,0557	45	0,00139	8	1,46686	1,88677	7	0,282559	14	0,282557422	-6,58369	0,93732	1,2	1,4	1,1	65	0
145	0,1217	97	0,00294	18	1,46675	1,88669	6	0,282375	15	0,282371869	-13,14627	1,27466	1,5	1,8	1,5	65	0